HHS Public Access

Author manuscript

Cell Rep. Author manuscript; available in PMC 2026 February 25.

Published in final edited form as:

Cell Rep. 2026 January 27; 45(1): 116730. doi:10.1016/j.celrep.2025.116730.

Convergent thyroid-ATPase interactions regulate collective behavior in *Danionella*

David Zada[1,2,4], **Mykola Kadobianskyi**[3,4], **Benjamin Judkewitz**[3], **Matthew Lovett-Barron**[1,5,*]

[1]Department of Neurobiology, School of Biological Sciences, University of California, San Diego, La Jolla, CA 92093, USA

[2]Gonda Multidisciplinary Brain Research Center, Bar-Ilan University, Ramat Gan 5290002, Israel

[3]Einstein Center for Neurosciences, Charité – Universitätsmedizin Berlin, Berlin, Germany

[4]These authors contributed equally

[5]Lead contact

SUMMARY

Collective behavior emerges from socially interacting individuals. Across species, the social behavior of healthy adults is often not present in immature animals, in socially isolated animals, or in animals with certain genetic perturbations, including models of autism spectrum disorder (ASD). Although social behavior is impaired in all these conditions, it remains unclear whether they act through shared or distinct genetic pathways. Here, we investigate the genetic regulators of collective schooling behavior in *Danionella cerebrum*, by applying RNA sequencing to the brains of animals with impaired or immature social behavior: juvenile animals, socially isolated adults, and ASD-related gene crispants. By comparing gene expression to controls, we identify a small set of differentially expressed genes common to these conditions, including thyroid signaling pathway, circadian rhythm-regulating genes, the transcription factor *klf9*, and the ATPase subunit *atp1a1a.4*. Genetic and pharmacological manipulations confirm their functional importance, demonstrating convergent molecular pathways regulating social interactions and collective behavior.

In brief

Zada, Kadobianskyi et al. develop methods for measuring and manipulating gene expression in the schooling glassfish *Danionella cerebrum*, identifying circadian genes and the thyroid-*klf9*-*atp1a1* pathway as commonly regulated across multiple models of impaired or immature collective behavior.

*Correspondence: mlb@ucsd.edu.

AUTHOR CONTRIBUTIONS

D.Z. and M.L.-B. designed the experiments. D.Z. conducted behavioral and molecular experiments. D.Z. and M.K. analyzed the data. B.J. and M.L.-B. supervised the research. D.Z., M.K., B.J., and M.L.-B. wrote the paper.

DECLARATION OF INTERESTS

The authors declare no competing interests.

DECLARATION OF GENERATIVE AI AND AI-ASSISTED TECHNOLOGIES IN THE WRITING PROCESS

NA.

Graphical Abstract

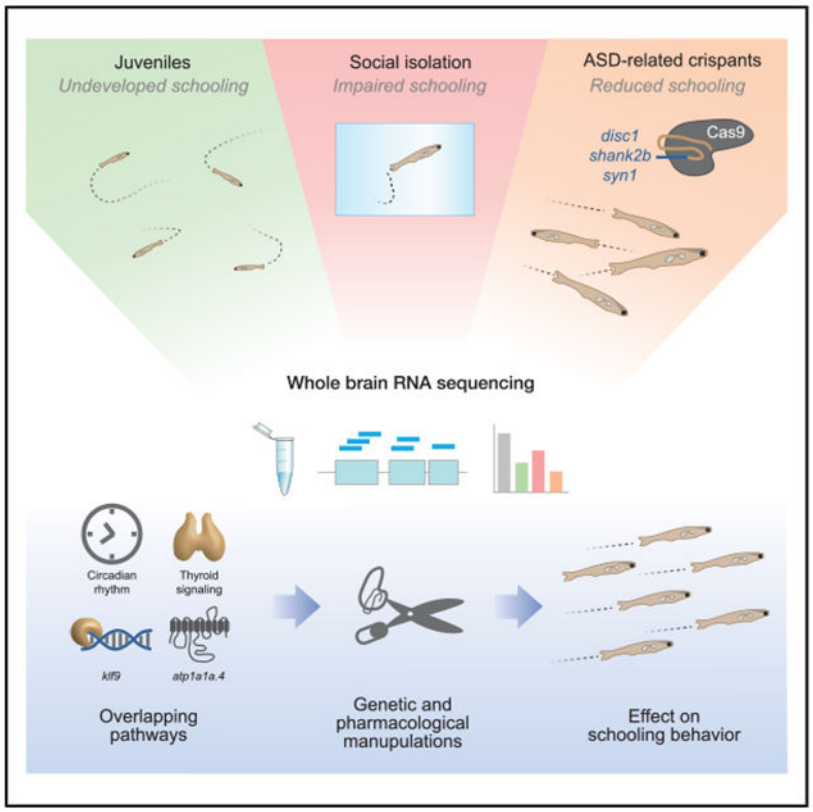

INTRODUCTION

Many animal species move in cohesive groups, where social interactions among individuals produce collective behavior.[1–4] Studies of fish schools have demonstrated that collective movement emerges from local interaction rules among group members, including short-range avoidance, long-range attraction, and postural alignment with neighbors[2,5–8]—social interactions that mature over development.[9–14] Social behaviors, including collective movement, are governed by numerous genetic and neural factors. Studies in humans and other mammals have identified several key genes involved in species-typical social behavior. For instance, mutations in genes such as *SHANK2*/*SHANK3* and *SYN* are linked to autism spectrum disorders (ASD),[15–17] and *DISC1* with both ASD and schizophrenia,[18,19] resulting in impaired social interactions. Studies in zebrafish have shown that mutations in genes encoding neuropeptides and their receptors impair social preference,[20–22] and comparative screens of ASD- and schizophrenia-related genes identified a variety of common behavioral, neuroanatomical, and activity phenotypes in larvae,[23,24] as well as impaired group behavior in adults.[25] However, adult zebrafish show less alignment than schooling fish species,[26] and thus the genetic contributions to collective movement and social interactions in schooling fish are not well understood.

The micro glassfish (*Danionella cerebrum*) is an emerging model system[14,27–33] that offers several advantages for investigating the genetic basis of social and collective behaviors. *D. cerebrum* are small and translucent, genetically tractable, and display visually based collective behavior, including the social aggregation and postural alignment typical of schooling.[14,27] Schooling emerges over the course of development in *D. cerebrum*, from social avoidance as larvae to coherent schooling as adults—a process that depends on social experience over development.[14] With these features, *D. cerebrum* is an attractive model system for studying how neural and genetic features of individuals contribute to the collective behaviors of groups,[34] and how social impairments in individuals impact group behavior.

In this study, we investigated the genetic basis of schooling and social development in *D. cerebrum*, using RNA sequencing (RNA-seq) of the brains of fish spanning multiple developmental stages, adults raised in social isolation, and fish with CRISPR-Cas9-mediated gene knockdown. This work provides insights into the genetics of social development, social dysfunction, and the collective behavior of groups.

RESULTS

Brain transcriptomes identify genes associated with social development

Collective behavior in *D. cerebrum* progresses from social avoidance at two weeks of age to aggregated and aligned schools at six weeks, where they reach sexual maturity and begin producing sound for acoustic communication.[14,35] Social isolation of *D. cerebrum* until six weeks of age results in impaired schooling and altered neural encoding of social motion.[14] To identify gene expression associated with typical social development, we dissected the brains of two- and six-week-old socially raised *D. cerebrum,* as well as six-week-old socially isolated *D. cerebrum*, and performed RNA-seq of whole brains, followed by DESeq2 analysis to identify differentially expressed genes (DEGs, Figure 1A; Table S1).

Comparing two- and six-week-old brains, 6,831 genes were upregulated (mean log2 fold-change [logFC] ~0.5) and 7,422 downregulated (mean logFC ~ −1.5, Figure 1B), from a total of 23,180 genes (after removing low count genes, see STAR Methods). Comparing socially raised versus isolated adult brains, 5378 genes were upregulated (mean logFC ~0.3) and 6434 downregulated (mean logFC ~ −1.3, Figure 1C). Since both two-week-old and six-week-old socially isolated groups exhibited reduced social interactions compared to typical adults, we next compared DEGs between them. A Venn diagram revealed that more than 50% of DEGs were shared between the two groups relative to the six-week-old control, with 3,289 upregulated and 5,041 downregulated genes (Figure 1D). This overlap in DEGs is significantly greater than expected by chance ($p < 0.0001$, hypergeometric test). Gene ontology (GO) analysis identified several brain development processes enriched and upregulated in two-week-old and in socially isolated fish compared to six-week-old fish, including regulation of presynapse assembly, axonogenesis, and brain development, among others (Figure 1E). In contrast, genes associated with antigen processing and presentation, immune response, major histocompatibility complex class II protein complex, lipoprotein metabolic processes, lipid transport, and lipid binding showed reduced expression, indicating downregulation of neuroimmune interactions and

lipid metabolism-related processes (Figure 1E). These changes suggest a potential role of neuroinflammation in the disruptions in social development.[36,37] These findings highlight the role of social experience in regulating gene expression underlying normal brain development.

Impaired schooling in crispants of ASD risk genes

To further investigate the genetic influences on collective behavior, we developed methods to manipulate ASD risk genes in *D. cerebrum*, targeting genes whose manipulations interfere with typical social behaviors in both rodents and zebrafish.[15,38] We used the CRISPR-Cas9 system to generate F0 *D. cerebrum* mutants—known as crispants[33,39,40]—targeting the *disc1*, *shank2b* (*D. cerebrum* ortholog of *SHANK2*), and *syn1* genes (Figures S1A and S1B). These three genes are involved in synaptic structure and function,[41–43] and their impairment is associated with neuropsychiatric disorders in humans.[16–19] To validate that these genes are conserved and expressed in the brain of *D. cerebrum*, we used whole-mount RNA *in situ* hybridization with hybridization chain reaction (HCR)[44] in two-week-old *D. cerebrum*, showing that *disc1*, *shank2b*, and *syn1* are widely expressed in the brain (Figure S1C; Table S2). RNA-seq data show that *disc1* expression remained stable throughout development but decreased in socially isolated six-week-old fish; *shank2b* was reduced in socially raised six-week-old brains relative to two-week-old and isolated fish; and *syn1* increased in six-week-old brains and further in socially isolated fish (Figure S1D). Injecting the Cas9-gRNA (guide RNA) ribonucleoprotein (RNP) complex into one-cell stage embryos resulted in 70%, 65%, and 90% crispants of *disc1*, *shank2b*, and *syn1*, respectively, characterized by depletion of the wild-type sequence and the emergence of alternative sequences at the target site (Figure S1B, see STAR Methods).

We measured collective movement in groups of four *disc1*-, *shank2b*-, or *syn1*-crispants, in addition to Cas9-only injected control adult *D. cerebrum* (Figure 2A). Compared to control groups (69.1 ± 8.5 mm/s), each ASD-related crispant fish moved more slowly by 19.76% (55.4 ± 10.1 mm/s, $p = 0.02$), 16.42% (57.7 ± 9.3 mm/s, $p = 0.03$) and 22.24% (53.7 ± 8.6 mm/s, $p = 0.002$ in *disc1*-, *shank2b*-, and *syn1*-crispants, respectively (Figure 2B).

We then quantified the aggregation and alignment of *D. cerebrum* groups. As described previously,[14] we quantified social aggregation by identifying the location of each social partner relative to the focal fish and the average area occupied by the group (Figure 2C). Aggregation was reduced in all ASD-related crispant fish compared to control groups (160.0 ± 42.4 mm^2), with the average area occupied by the group increasing by 73.85% (278.2 ± 57.2 mm^2, $p = 0.00092$), 66.97% (267.2 ± 99.4 mm^2, $p = 0.022$), and 120.21% (352.4 ± 90.6 mm^2, $p = 8.4 \times 10^{-5}$, Figure 2D) in *disc1*-, *shank2b*-, and *syn1*-crispants, respectively. We next examined the postural alignment by characterizing the difference in heading angle between each fish and its nearest neighbor. Crispant groups were less aligned to each other compared to Cas9-only control fish (Figure 2E), with a decrease in the mean Pearson's correlation coefficient between group member headings by 66.47% ($r = 0.14 \pm 0.13$, $p = 0.0012$), 63.13% ($r = 0.16 \pm 0.13$, $p = 0.0018$), and 81.9% ($r = 0.078 \pm 0.08$, $p = 4.6 \times 10^{-6}$) in *disc1*-, *shank2b*-, and *syn1*-crispants, respectively, compared to control groups ($r = 0.43$

± 0.12, Figure 2F). These results indicate that mutations in ASD-related risk genes reduce schooling behavior in adult *D. cerebrum*.

Comparison of ASD-related crispant transcriptomes reveals common DEGs

To investigate gene expression in ASD-related *D. cerebrum* models, we performed RNA-seq on brains from crispants and Cas9-only control groups. Volcano plots of ASD-related crispants reveal 1,211 upregulated and 612 downregulated DEGs in *disc1* crispants, 2,717 upregulated and 2,639 downregulated DEGs in *shank2b* crispants, and 282 upregulated and 581 downregulated DEGs in *syn1* crispants (Figures 2G–2I). Comparative analysis across the different groups identifies 706 upregulated and 265 downregulated unique DEGs in *disc1* crispants, 2,254 upregulated and 2,304 downregulated unique DEGs in *shank2b* crispants, and 74 upregulated and 239 downregulated unique DEGs in *syn1* crispants (Figure 2J).

We next examined convergently regulated genes across all crispant groups and identified 108 upregulated and 50 downregulated DEGs (Figures 2J and S2). GO enrichment analysis of these genes revealed that the main impacted pathways were related to circadian rhythms, including negative regulation of circadian rhythm, circadian rhythm, and circadian regulation of gene expression (Figure 2K). Similar to the results from two-week-old and socially isolated brains, we observed increased expression of circadian-related genes such as *cipc*, *per1*, *bhlhe41*, and the transcriptional regulators *tef* and *nr1d1*, along with reduced expression of *cry1* and *arntl* (Table S1).

To examine the functional consequences of these disruptions on circadian-related genes in ASD-related crispants, we tested groups of heterozygous F1 *shank2b*$^{+/-}$ mutant *D. cerebrum*. The Shank2b protein consists of 1,762 amino acids predicted to include the main SHANK protein domains; *shank2b*$^{+/-}$ fish harbored a 22-bp deletion that resulted in a frameshift and the incorporation of a premature termination codon at amino acid 57, predicted to produce a truncated protein (Figure S3A). We monitored the circadian behavior of *shank2b*$^{+/-}$ fish and their wild-type (WT) siblings for 24 h under normal light/dark conditions (see STAR Methods).

To validate that both *shank2b*-crispants and *shank2b*$^{+/-}$ fish exhibit similar behavioral phenotypes, we analyzed schooling behavior at two time points during daytime (beginning and end of daylight). Similar to *shank2b*-crispants, *shank2b*$^{+/-}$ fish demonstrated reduced speed by 22% (WT siblings: 57.23 ± 5.8 mm/s, *shank2b*$^{+/-}$: 44.64 ± 7.5 mm/s, $p = 0.006$), reduced heading correlation by 46.2% (WT siblings: 0.26 ± 0.08, *shank2b*$^{+/-}$: 0.14 ± 0.04, $p = 0.01$), and increased group area by 38.2% (WT siblings: 222.4 ± 38.37 mm^2, *shank2b*$^{+/-}$: 307.87 ± 65.44 mm^2, $p = 0.015$), indicating reduced schooling (Figures S3B–S3D). Locomotor activity of WT fish peaked during the daytime (day: 23.76 ± 2.3 mm/s), decreased during nighttime (night: 13.01 ± 0.9 mm/s), and slightly increased back during the following daytime under dark conditions (subjective day: 17.4 ± 1.6 mm/s, $H = 14.84$, $p = 0.0006$, Figure S3E), showing diurnal rhythms of *D. cerebrum*. In contrast, *shank2b*$^{+/-}$ fish exhibited similar locomotor activity during day and night as well as subjective day (day: 21.8 ± 2.7 mm/s, night: 17.93 ± 1.78 mm/s, subjective day: 15.34 ± 1.68 mm/s, $p = 0.19$, Figure S3F). These findings suggest that circadian rhythms are disrupted in a *D. cerebrum*

model of an ASD risk gene and highlight that circadian regulation correlates with brain development and social behaviors.

Comparison across different classes of social development disruptions

With DEGs identified across development, social isolation, and three ASD crispant models, we next analyzed commonly up- or downregulated genes compared to typical schooling adults, in order to identify candidate pathways involved in collective behavior. We first compared DEGs across ASD-related crispants and socially isolated fish, and found 40 upregulated and 5 downregulated DEGs (Figure 3A). The downregulated DEGs include the sodium/potassium-transporting ATPase subunit α1, tandem duplicate 4 (*atp1a1a.4*), calreticulin (*calr*), serpin H1 (*serpinh1*), and two variants of the nuclear receptor Ror (*rorb* [*hr46*] and *rorc*)—genes important for cellular function and neurodevelopment (Figure 3B). Many upregulated DEGs relate to synaptic structure and function, including *slc17a7 (vglut1)*, *rapgefl1*, *dlgap2*, *camk4*, *ngef*, *ldb1*, *bhlhe40*, *cacnb2*, *glra2*, and *abi2* (Figure 3B). Additionally, *itm2c*, which is involved in the negative regulation of neuron projection, plays a role in neuron differentiation. Together with *ldb1*, *rapgefl1*, *camk1*, *ngef*, and *vegfa*—genes enriched in nervous system development GO terms (Figure 3B)—these findings suggest the presence of delayed neural development and/or compensatory mechanisms in these models, associated with synaptic abnormalities found in ASD.[45]

Genes related to circadian functions are also found among common DEGs, including downregulated *rorb* and *rorc*, and upregulated *tef* and *bhlhe40*; *rorb* and *rorc* ensure the rhythmic expression of *bmal1*,[46] *tef* is influenced by core circadian machinery and regulates the rhythmic expression of downstream target genes,[47] while *bhlhe40* (also known as Dec1) is a repressor within the circadian feedback loop that modulates gene expression involved in metabolism and hormonal regulation[48] (Figure 3B).

Interestingly, we found thyroid-related genes differentially expressed across these social dysfunction models. Among commonly upregulated genes, we identified the transcription factor *tef*, which regulates thyroid-stimulating hormone beta (Tshb),[49] and *iodothyronine deiodinase 2* (*dio2*), which converts the prohormone thyroxine (T4) into the bioactive thyroid hormone triiodothyronine (T3).[50] This suggests potentially increased thyroid hormone levels in the brains of these social dysfunction models. Furthermore, the *klf9* gene, a transcription factor known to regulate neurogenesis and to be induced by thyroid hormone,[51] was also among upregulated DEGs (Figure 3B).

One consideration is that chronic stress during development may contribute to the gene expression changes observed in ASD-related crispants and isolated fish.[52,53] We examined this possibility by comparing DEGs between adults and two-week-old fish, which do not school[14] but have not undergone interventions that could induce stress. Among the DEGs common to socially isolated fish and the three crispants, we identified 12 genes that were not differentially regulated in two-week olds, including *slc17a7a*, *slc20a1b*, *vipr1*, and *dio2* (underlined in Figure 3B). These genes are associated with chronic stress phenotypes,[54–57] suggesting stress may underlie some of the behavioral abnormalities seen in crispants and socially isolated fish. However, the other genes common to all these conditions—including

those associated with circadian rhythm and thyroid function—suggest important roles of these processes in the social development of *D. cerebrum*.

Thyroid hormone and *klf9* regulate *atp1a1a.4* mRNA expression

We next sought to investigate the most significant commonly downregulated gene: *atp1a1a.4*. We investigated whether there is a relationship between this gene and upregulated DEGs, as well as its functional link to collective schooling behavior. In mammals, *atp1a1* is regulated by various transcription factors, including specificity protein 1 (*sp1*).[58] Although *sp1* itself is not a DEG in our datasets, the SP1-like transcription factor *klf9* is among the top upregulated DEGs; KLF9 is a transcriptional repressor, whereas SP1 acts as a transcriptional activator.[59] To validate that these genes are also differentially expressed in *shank2b*$^{+/-}$ fish, we measured their expression in the brains of F1 *shank2b*$^{+/-}$ fish with quantitative reverse-transcription PCR (RT-qPCR). Similar to *shank2b*-crispants, *klf9* mRNA levels increased by 99.1% ($p = 0.034$), and *atp1a1a.4* mRNA decreased by 82.6% ($p = 0.013$) in *shank2b*$^{+/-}$ fish compared to WT siblings (Figures S4A and S4B).

We next examined the link between *klf9* and *atp1a1a.4*. Using HCR *in situ* hybridization, we found widespread expression of these genes in the *D. cerebrum* brain, with prominent midline expression of *klf9* in two-week-old fish and co-labeling of *klf9* and *atp1a1a.4* in adults (Figures 4A and 4B; Table S2). To test whether *klf9* inhibits *atp1a1a.4* transcription in *D. cerebrum*, we used an inducible heat-shock promoter to overexpress *klf9*. We co-injected embryos with a *pTol2-hsp70:klf9* construct and *transposase* (*TP*) mRNA (or only *TP* mRNA for control), and subjected 4 days post-fertilization (dpf) larvae to one hour of heat shock on two consecutive days. At 6 dpf, we measured the expression levels of *klf9* and *atp1a1a.4* with RT-qPCR. Compared to heat-shocked controls, *klf9* mRNA levels increased by 101% in *pTol2-hsp70:klf9*-injected larvae ($p = 0.0006$, Figure 4C), and *atp1a1a.4* expression was reduced by 78% ($p = 0.02$, Figure 4D). We therefore conclude that increased *klf9* suppresses *atp1a1a.4* expression in the *D. cerebrum* brain.

Since increased levels of *tef* and *dio2* suggest increased levels of T3, and *klf9* is known to be regulated by thyroid hormone,[60,61] we next examined whether T3 influences the expression of *klf9* and *atp1a1a.4*. We treated *D. cerebrum* larvae with 10 nM T3 beginning at 3 dpf for three consecutive days,[62] then measured transcript levels of *klf9* and *atp1a1a.4* with RT-qPCR at 6 dpf. While *klf9* expression levels increased by 44% ($p = 0.005$, Figure 4E), *atp1a1a.4* expression levels decreased by 22% under T3 administration ($p = 0.02$, Figure 4F). These findings build upon our transcriptomic comparisons to identify a causal link between thyroid hormone, *klf9*, and *atp1a1a.4* in *D. cerebrum,* as potential genetic regulators of their collective schooling behavior.

Thyroid hormone treatment reduces schooling behavior

To test the effect of thyroid hormone on schooling, we recorded the behavior of groups of four adult *D. cerebrum*, treated them with T3 (50 nM or NaOH vehicle control) for three consecutive days, then monitored their behavior again (Figure 4G). While swimming speed remained similar across groups before and after treatment (Figure 4H), and neither group area nor heading correlation were changed in vehicle-treated fish (Figures 4I and 4J), we

observed schooling differences in the T3-treated group. Specifically, group area increased by 236.8% (Pre-T3: 315.7 ± 41.2 mm^2; Post-T3: 1063.64 ± 141.4 mm^2, $p = 9 \times 10^{-5}$, Figure 4I), and heading correlation decreased by 97.3% (Pre-T3: $r = 0.32 \pm 0.07$; Post-T3: $r = 0.008 \pm 0.019$, $p = 0.0002$, Figure 4J).

Following behavioral monitoring, we collected the brains of these fish to assess whether T3 treatment altered *klf9* and *atp1a1a.4* expression using RT-qPCR. *klf9* expression was increased by 90% (p-adjusted = 0.3) in 50 nM T3-treated fish, and by 329% (p-adjusted = 0.02) in 100 nM T3-treated fish (Figure S4C). In addition, *atp1a1a.4* expression decreased by 44% (p-adjusted = 0.04) and 90% (p-adjusted = 0.001) in 50 nM and 100 nM T3-treated fish, respectively (Figure S4D). These results show that thyroid hormone influences the expression of *klf9* and *atp1a1a.4,* and regulates schooling behavior in *D. cerebrum*.

Schooling behavior is impaired in *atp1a1a.4* crispants

The reduced expression of *atp1a1a.4* across all social dysfunction models suggest that this gene may play an important role in collective schooling behavior. To test this hypothesis, we used CRISPR-Cas9 to knock down the *atp1a1a.4* gene (*atp1a1a.4*-crispants, Figure 4K). Injecting one-cell stage embryos with the *atp1a1a.4* RNP complex resulted in 85% crispants, as detected by reduction in the wild-type sequence and the appearance of variant sequences at the target site. We recorded groups of four adult fish and tracked the position and body orientation of individual fish to quantify the speed, aggregation, and alignment of *atp1a1a.4*- crispants and Cas9-only injected controls. In contrast to ASD-related crispants, *atp1a1a.4*- crispants swam faster than controls by 10.92% (control: 52.5 ± 5.7 mm/s, *atp1a1a.4*: 58.23 ± 5.1 mm/s, $p = 0.046$; Figure 4L). However, similar to ASD gene crispants, *atp1a1a.4* crispants exhibited reduced schooling behavior; group area increased by 128.35% in crispants (i.e., reduced aggregation; control: 129.0 ± 8.9 mm^2, *atp1a1a.4*: 294.6 ± 86.5 mm^2, $p = 0.0005$; Figure 4M) and heading correlation was reduced by 47.19% (i.e., reduced alignment; control: $r = 0.39 \pm 0.14$, *atp1a1a.4*: $r = 0.2 \pm 0.07$, $p = 0.013$) compared to control-injected fish (Figure 4N). These results indicate that *atp1a1a.4* is a key factor for schooling behavior in *D. cerebrum*, and is commonly impaired across multiple models of social dysfunction.

DISCUSSION

Collective movement and other social behaviors emerge over the course of development,[9–14] driven by the extensive genetic and molecular changes in maturing nervous systems. Disruptions to these processes, whether caused by genetic mutations or environmental factors, can impair the functioning of critical genes involved in neurodevelopment and social behavior.[63,64] In this study, we used *D. cerebrum* as a model system to investigate the differences in gene expression between highly social adults and fish that do not school: juvenile fish, three ASD-related crispant models, and adults raised in social isolation. By comparing brain transcript levels across these conditions, we observed considerable differences in the genetic pathways affected by each perturbation. Despite such differences, we identified a set of commonly regulated pathways related to circadian rhythms and thyroid hormone signaling as regulators of collective social behavior. This approach

revealed that the thyroid-*klf9*-*atp1a1* pathway—previously examined in development and homeostasis[51,60–62,65,66]—is commonly modulated in models of impaired collective behavior. By demonstrating that experimental manipulations of this pathway alter schooling in *D. cerebrum*, our work suggests a role for this pathway in the development and expression of collective social behavior.

Circadian rhythms maintain sleep-wake cycles and physiological processes, and their disruption has been linked to impaired social behavior and mental health in humans.[67–69] Social interactions help synchronize circadian rhythms across species, including primates,[70] rodents,[71] and insects.[72] For instance, social isolation in rodents alters the expression of circadian genes and sleep,[73,74] and group interactions stabilize behavioral rhythms in animal collectives.[75] Our findings support the idea of phase shifts in circadian rhythms between juvenile and adult fish,[76] suggesting that genetic and social disruptions can lead to circadian dysregulation and immature social behavior. Another option is that ASD-related mutations cause sleep disturbances,[77] which interfere with circadian rhythms, and thus social engagement. Altogether, this highlights the interplay between circadian regulation of the brain and the development of social behavior.

Thyroid hormone signaling also influences neurodevelopment, with T3 and T4 regulating neurogenesis, synaptic plasticity, and neural circuit maturation.[65] Disruptions in thyroid signaling have been implicated in neurodevelopmental disorders,[62,78] including ASD, where altered hormone levels are associated with cognitive and social deficits.[79] Here, we show that elevated T3 levels in the brain can lead to impaired collective behavior through changes in gene expression. Thyroid signaling may be engaged during neurogenesis[80] induced by neurodevelopmental alterations or could act as a compensatory mechanism in response to such disruptions. Elevated thyroid hormone levels have been observed in animal models exposed to prenatal stress,[81] potentially as a buffer against neurodevelopmental stress to influence processes related to neural and behavioral development. Thyroid hormones also regulate morphogenesis and tissue differentiation across species[82–84]; however, we observed no gross morphological alterations in socially impaired *D. cerebrum*, suggesting a more specific role for thyroid signaling in neurodevelopment and social behavior in our models via increased expression of the thyroid hormone-responsive transcription factor *klf9*.[51,60,61]

We found that *klf9* and *atp1a1a.4* are widely co-expressed across the brain in both juvenile and adult *D. cerebrum*, and that increased *klf9* levels repress the expression of *atp1a1a.4*—an ATPase subunit that contributes to maintaining transmembrane ion gradients. We found that directly reducing the expression of *atp1a1a.4* impairs collective schooling behavior, and prior work has also linked *atp1a1* abnormalities to behavioral impairments, including major depressive disorder,[85] as well as sensory motor neuropathies, hypomagnesemia, seizures, and cognitive delay.[86] Beyond its role in neuronal excitability, *atp1a1* contributes to brain development by supporting neuroepithelial organization and ventricle formation. Studies in zebrafish have shown that *atp1a1*, together with *fxyd1* and *cldn5a*, are essential for brain ventricle expansion, neuroepithelial barrier integrity, and morphogenesis.[66,87,88] Furthermore, *klf9* regulates transcription related to hippocampal neurogenesis and stem cell expansion in mice.[89,90] Thus, disruptions in this thyroid-*klf9*-*atp1a1a.4* signaling pathway

could influence not only neuronal circuit function but also brain morphogenesis and homeostasis.

In conclusion, our findings emphasize the importance of circadian rhythm regulation and thyroid hormone signaling in the development of collective behavior in schooling fish. While ASD-related genetic disruptions and social isolation influenced many disparate genetic targets, we found convergent alterations of a subset of genetic pathways, including the thyroid-*klf9-atp1a1* pathway. These data provide insight into the genetic and molecular mechanisms underlying the collective behavior of animals in groups and provide opportunities for using this model system to examine how molecular pathways shape the development and function of the social brain.

Limitations of the study

This work was designed to be a genetic entry point into the biology of collective schooling in *D. cerebrum*, and we acknowledge several key limitations. First, our transcriptomic analyses relied on bulk RNA-seq of whole brains, rather than region-specific or single-cell RNA-seq. Therefore, we cannot assign gene expression to cell types or circuits, which will require future studies using single-cell and/or spatial transcriptomics. Second, while we validated the functional impact of a known thyroid-*klf9-atp1a1* pathway on schooling, their mechanistic interactions are not yet completely mapped in *D. cerebrum*. Future work can identify intermediate regulatory elements, direct KLF9 binding partners, and the circuit nodes through which the regulation of ATPase expression influences collective behavior. Third, we used F0 crispants for genetic manipulations, which can introduce variation in mutations across individuals. Although we used a single gRNA to target each gene and sequenced each individual, we cannot exclude the possibility of off-target edits that may add variance and obscure dose-dependent effects in such models. These limitations and others can be addressed through further methods development for *D. cerebrum*,[91] including spatially resolved transcriptomics, behavioral and hormonal assays, and methods for cell-type- and circuit-specific genome editing.

RESOURCE AVAILABILITY

Lead contact

Further information and requests for resources should be directed to and will be fulfilled by the lead contact, Matthew Lovett-Barron (mlb@ucsd.edu).

Materials availability

Materials are available from the lead contact upon request.

STAR★METHODS

EXPERIMENTAL MODEL AND STUDY PARTICIPANT DETAILS

The behavioral and molecular experiments with *D. cerebrum* were approved by the government authorities (U.S. Animal Care, and Institutional Animal Care and Use Committee (IACUC), (USDA Registration Number 93-R-0437)) and carried out in

accordance with the U.S. federal and California state law to enforce the Animal Welfare Act (AWA) under the California Health and Safety Code. *D. cerebrum* aged between 2 weeks post fertilization and adults (~1 year) were used in the experiments. These animals were either WT, F0 crispants, or F1 *shank2b*+/− genotypes. Adult *D. cerebrum* were both males and females in our studies.

METHOD DETAILS

Fish husbandry: *D. cerebrum* were raised and maintained in standard zebrafish housing systems (Aquaneering) under controlled conditions: system water temperature of 28 ± 0.5°C, pH 7.0, and conductivity of 525 μS/cm. The fish were kept on a 14-h light/10-h dark cycle and fed twice daily. Breeding was carried out in communal tanks containing 20–40 individuals, with ~5 cm silicone tubes provided as spawning sites. Eggs were collected during the first hour of daylight and 1–2 h following morning and afternoon feedings. Embryos (0–5 days post-fertilization) were reared in egg water (0.2 mg/L Instant Ocean, 3 g/L $CHNaO_3$, and 0.15% methylene blue dissolved in reverse osmosis-purified water) inside an incubator set to 29 ± 0.5° C. Larvae (5–14 days post-fertilization) were cocultured with L-type rotifers (*Brachionus plicatilis*) in static tanks, where the water level was increased by approximately 1 L per day. At 14 days old, after being transferred to a circulating water system, *D. cerebrum* were fed progressively larger quantities of *Artemia*. For isolation experiments, single fish were housed in individual tanks separated by visual barriers. Isolation began after hatching from the chorion at 2–4 days post-fertilization.

Cas9-CRISPR-based crispants and microinjection: To generate *disc1*, *shank2b*, *syn1*, and *atp1a1a.4* crispants, we used a modified CRISPR/Cas9 protocol similar to previously described methods.[33,39,40] sgRNAs were designed and synthesized by IDT (Alt-R CRISPR-Cas9 System), for *disc1* (sgRNA site: 5′-CTCAAGAGTTGTGTGACAAG-3′), *shank2b* (sgRNA site: 5′-GACAATCTGTGTGGTTATCC-3′), *syn1* (sgRNA site: 5′-GAGATCGCC CATATATCCAT-3′) and *atp1a1a.4* (sgRNA site: 5′-AGTATGGTACTGACCTCACC-3′) The sgRNA's were diluted in IDTE buffer to 100 mM stock solution, according to the manufacturer's protocol. Pre-assembled RNPs composed of Cas9 protein and sgRNA are highly effective in zebrafish.[39,40] Therefore, RNPs generated before the microinjection by mixing 4 mg/mL of Alt-R S.p. Cas9 Nuclease V3 (IDT) and 600 ng/mL of each sgRNA, incubated at 37°C for 5 min, and chilled in ice-cold water. For control groups we injected only 4 mg/mL of Alt-R S.p. Cas9 Nuclease. The expression of the RNPs were performed by microinjection of approximately 2 nL of each solution into one-cell-stage embryos, using a micromanipulator and the FemtoJet 4i microinjector (Eppendorf 5252000021). All injections were performed within the same week, and on each injection day both crispant and Cas9-only control fish were injected in parallel.

To assess the efficiency of each RNP injection, we sampled ten larvae from each injected group. Genomic DNA was extracted by placing individual larvae into 100 μL of 50 mM NaOH and incubating the mixture at 95°C for 10 min. After chilling on ice for 5 min, 10 μL of Tris-HCl (pH 8.0) was added, followed by vortexing for 10 s and centrifugation for 2 min at 12,000 rpm. The genomic DNA was amplified by PCR using the following primers: *disc1*: 5′-TTCAAATTGTAGAGTCTGCTTTAAG-3′ and 5′-

GTGGTGATCACAGGAGGAGT-3′, *shank2b*: 5′ -ATGATGCCACGAAGCCCCAT-3′ and 5′-GAGATCTCCACCACTCACTTCT-3′, *syn1*: 5′-CAGTCCGTCTGCTGGTCATCA-3′ and 5′-GTGTAATTTGTCCTGCAAAACAGGG-3′, *atp1a1a.4*: 5′-GGCTGCAACTTCAGATGATGG-3′ and 5′-AGCTGCAAGTTCCTTGACGA-3′. The resulting amplicons—353 bp for *disc1*, 264 bp for *shank2b*, 367 bp for *syn1*, and 446 bp for *atp1a1a.4*—were sequenced using Sanger sequencing (Azenta Life Sciences, San Diego). Fish showing notable depletion of the wild-type peak and the appearance of alternative peaks at the target site were classified as crispants (Figures S1A and S1B). We found that RNP injections for *disc1*, *shank2b*, *syn1* and *atp1a1a.4* resulted in 70%, 60%, 90%, 90% crispants, respectively. Following behavioral experiments in adult fish, tail-clip samples were taken to confirm the presence of crispants in the tested groups. The ratios of crispants remained similar, with 70%, 70%, 90% and 80% crispants in the *disc1*-, *shank2b*-, *syn1* and *atp1a1a.4*-injected groups, respectively. Overall, the efficiency was 70%, 65%, 90% and 85% crispants (fish that possess notable depletion of the wild-type peak) in the *disc1*-, *shank2b*-, *syn1* and *atp1a1a.4*-injected groups, respectively.

The injected crispants (F0) were raised to adulthood and outcrossed with WT *D. cerebrum*. We attempted to establish stable lines for *disc1* and *syn1*, but failed to obtain F1 offspring. We did obtain F1 *shank2b*+/− fish, which were raised to adulthood and identified as heterozygotes or WT siblings using tail-clip genotyping. These F1 fish were used for the experiments. We attempted to obtain F2 progeny by outcrossing *shank2b*+/− fish with WT, and with inbreeding amongst *shank2b* +/− individuals, but these efforts were unsuccessful.

Heat shock experiments: *pTol2-hsp70:klf9* was generated using the Gateway cloning system. Briefly, the full *klf9* coding sequence was amplified by PCR with the primers 5′-AAGGTCGACATGACCACAATGACGGACGT-3′ and 5′-ACCAAGCTTTCAGAGCCCTCCATTTGAGTG-3′. The PCR fragment and the *pME-MCS* vector were digested with *SalI*-HF and *HindIII*-HF restriction enzymes (NEB) and then ligated using *T4* DNA ligase (NEB) to generate *pME-klf9*. For the final plasmid (*pTol2-hsp70:klf9*), the entry vectors *p5E-hsp70L*, *pME-klf9*, and *p3E-polyA* were transferred into the destination vector *pDestTol2CG2* using the Gateway LR Clonase reaction (Invitrogen 11791020).

To increase expression, *pTol2-hsp70:klf9* (20 ng/μL) was co-injected with *TP* mRNA (10 ng/μL) into one-cell-stage embryos. As a control, embryos were injected with *TP* mRNA (10 ng/μL) alone. At 5 dpf, larvae with EGFP-positive hearts and control larvae were transferred to pre-warmed 38°C water and incubated at 38°C for one hour. Following the heat shock, the larvae were immediately returned to a 28°C incubator. At 6 dpf, this treatment was repeated, and after one hour of recovery at 28°C, the larvae were sampled, and RNA was extracted.

Pharmacological experiments: In pharmacological assays, similar to previous works,[62,95] 3 dpf larvae were placed in Petri dishes (~40 larvae per dish) containing either 10 nM T3 or 5×10^{-6} M NaOH diluted in system water. The exposure medium (25 mL per dish) was exchanged twice daily. We used higher doses for adults, where groups of four adult fish were placed in a glass beaker containing either 50 nM or 100 nM T3, or 5×10^{-6} M NaOH diluted in 1 L of system water. Twice a day, the fish were fed, and the medium was

exchanged. Stock solutions of 100 mM T3 (Sigma-Aldrich, St. Louis, MO) were prepared in 0.05 M NaOH and diluted in housing water to the final administered concentrations. Although *klf9* and *atp1a1a.4* expression levels change with a higher fold-change in fish treated with 100 nM T3 compared to those treated with 50 nM T3 (Figure S4), they also exhibit abnormal morphology (swollen swim bladder) and baseline swimming and were therefore excluded from the behavioral experiments.

RNA extraction, cDNA and RT-qPCR: All samples were taken between 3 and 4 zeitgeber time and fish were not fed before. Total RNA was extracted from two-, four-, six-week-old and adult brains or 6 dpf larvae using the Direct-zol RNA MiniPrep kit (Zymo Research Corporation), according to the manufacturer's instructions. For whole brain RNAseq, for each tested group, a total of three biological samples, each containing four brains, were used. For measuring RNA expression levels in larvae and adults, four-six biological samples from each group were used. Each biological sample contained a pool of 10 larvae or 4 brains of adult fish. mRNA (500 μg) was reverse-transcribed using qScript cDNA SuperMix (Quanta BioSciences). Relative mRNA quantification of *klf9* and *atp1a1a.4* was determined using RT-qPCR. Relative transcript levels were determined by the CFX Opus 384 Real-Time PCR System (BIO-RAD). Triplicates of each cDNA sample were PCR-amplified using the PerfeCTa SYBR Green FastMix (Quanta BioSciences) and the following specific primers: *klf9*: 5′-GTGGCAAAGTCTACGGAAAATC-3′ and 5′-GGTATGTGTACGGAAGTGTCG-3′; *atp1a1a.4*: 5′-ACCACAAGTTGACACTCGATG-3′ and 5′-GAACTTGACCCATTCTGGAGTAG-3′ and the reference gene *mrpl13*: 5′-AGAGAAGGCGATATGTTTGGTG-3′ and 5′-CCTGGGAAAATCGCTTCATTG-3′; The relative quantification of each gene expression was normalized against *mrpl13* mRNA expression levels and subjected to the ΔΔCT method.

HCR staining and imaging: Pools of probes for *disc1, shank2b, syn1, klf9* and *atp1a1a.4* were ordered from IDT (Table S2), to match with the B1-Alexa 594, B2-Alexa 647, or B3-Alexa 647 amplifiers purchased from Molecular Instruments. Juvenile or adult fish were sacrificed and exsanguinated by first immersing them in ice-cold water and then placing them into 1X PBS with 0.5M EDTA added and then removing their tail. The fish were then fixed in 4% formaldehyde in PBS at 4°C for 24 h. Next, in adults, the skin on their head was pierced and they were cleared and permeabilized in a detergent solution (1X PBS, 1% Triton X-100, 0.2% SDS, 20 mM sodium sulfite) at 25°C for 48 h. Afterward they were washed in 1X PBS for 4 h and stained using a modified HCR protocol[44] for whole-mount samples. Briefly, after two 20-min 2X SSCT (2X SSC, 0.1% Tween 20) washes, the hybridization probes were added to each fish at 1:250 dilution in fresh hybridization buffer (2X SSC, 10% formamide, 10% dextran sulfate). The hybridization was conducted at 37°C for 20 h. Afterward, the samples were washed 3 times in 2X SSCT +30% formamide at 37°C and 2 times in 2X SSCT at 24°C, 20 min each. Afterward, they were incubated in the amplification buffer (5X SSCT, 10% dextran sulfate) while the fluorescent hairpins were heated to 95°C in the PCR machine and then snap cooled on ice. Hairpins were then allowed to return to room temperature for 20 min in a dark drawer and added to the samples in the fresh amplification buffer (4 μL of each hairpin to 50 μL of amplification buffer). The samples were left at room temperature overnight, washed 3 times for 30 min in 5X

SSCT and optically cleared in ~300 μL of RIMS for at least 24 h (EasyIndex custom RI 1.465, LifeCanvas Technologies). Finally, the samples were embedded in Sylgard molds and imaged using a custom two-photon microscope with a Nikon 16X NA 0.8 objective at 820 nm excitation wavelength.

Behavioral experiments: As previously described,[14] all behavioral experiments were controlled using BonsaiRx (bonsai-rx.org) with the BonVision and BonZeb packages.[93,96] The experiments were conducted in a dedicated behavioral room maintained at 28°C with central circulation and a portable electric heater. Each experimental group consisted of a mix of adult males and females (older than 8 weeks). The fish were tested in a transparent acrylic circular arena (300 mm diameter) with black walls and a transparent bottom lined with white styrene to diffuse light. The arena was filled with 1 L of system water and enclosed with black curtains to control ambient lighting conditions. The arena was illuminated with bottom-projected white light (AnyBeam Pico Projector, HD301M1-H2) and infrared light (CM-IR130-850NM, CMVision Technologies Inc.). Behavioral videos were recorded using a top-mounted camera (FLIR Grasshopper, #33–534) equipped with an 8 mm F/1.8 lens (Edmund Optics, #15–626) and a long-pass filter (Edmund Optics, #12–767). The videos were captured at a frame rate of 121 Hz. Behavioral activity recordings were taken between zeitgeber time 3 and 4, and fish were not fed before. Before recording, fish were habituated in the arena for 10 min. Recording started only after all fish were observed swimming without exhibiting freezing behavior, and their behavior was then recorded for 5 min.

In the 24-h light-dark-dark behavioral recording, fish were fed before the experiments began. They remained in the arena for the entire 24-h experiment, but recordings were conducted for 5 min every hour at the half-hour mark.

Behavior analysis: As described previously,[14] we used Social LEAP-Estimates Animal Poses (SLEAP[92]), to track fish location and posture in groups. Videos were manually proofread after pose inference, and output files (.h5) were analyzed using Python Colab notebooks.[14] The SLEAP model tracked six points per fish (nose to proximal tail, excluding the distal tail). The centroid (front of the swim bladder), nose (midpoint between eyes), and tail tip (second-to-last point) were used to calculate heading angle (vector from centroid to nose). Coordinates were converted from pixels to millimeters, and all data were smoothed with running averages (5-frame for x/y and 10-frame for speed). Nearest neighbors and their heading angle differences were identified at each time point. Fraction time moving (>2 body lengths/s), heading angle correlation (average pairwise Pearson correlation), and group area (convex hull) were calculated. For occupancy maps, the focal fish centroid was placed at the center of a 100 × 100 grid (100 mm^2 or 6 body $lengths^2$) oriented north, with other fish centroids displaced and rotated relative to the focal fish. Pixels with other fish present were assigned a value of 1, and the grid was down-sampled to 50 × 50 and summed.

Whole brain RNAseq: Three replicates were sequenced, each containing four brains. Behavioral results for the developmental stages and social isolation experiments were published in Zada et al.[14] and behavioral results for the ASD-related crispant fish and their control are presented in this study. We dissected the brains and stored them immediately at −80°C. After finishing sampling all brains of all groups, we used the Direct-zol RNA

MiniPrep kit (Zymo Research Corporation) to extract RNA. Total RNA was assessed for quality using an Agilent Tapestation 4200, and 100 ng of RNA from samples with an RNA Integrity Number (RIN) greater than 8.0 were used to generate RNA sequencing libraries using the Illumina Stranded mRNA Prep (Illumina). Samples were processed following manufacturer's instructions. Resulting libraries were multiplexed and sequenced with 100 bp Paired End reads (PE100) to a depth of approximately 25 million reads per sample on an Illumina NovaSeq 6000. Samples were demultiplexed using bcl2fastq Conversion Software (Illumina).

QUANTIFICATION AND STATISTICAL ANALYSIS

RNAseq and bioinformatics analysis: Obtained RNA sequencing libraries were first used to update the published *D. cerebrum* transcriptome annotation,[28] using funannotate update and funannotate interproscan pipelines (github.com/nextgenusfs/funannotate) as described previously.[97] Expression counts were obtained using salmon in the mapping mode.[98] Differential expression analysis of all samples has been performed in R using DESeq2.[94] Gene counts were filtered to discard counts ≤ 10 TPM. For all pairwise contrasts across the crispants and the socially isolated fish, alpha threshold was set to 0.05 and log-fold change threshold to 0. Gene Ontology enrichment analysis was done using goseq.[99] Zebrafish orthologues of *D. cerebrum* genes were additionally identified using reciprocal best hit BLAST (RBH) with the proteomes of the two species.

For information about protein/gene functions and pathways across the manuscript we manually collected data from https://www.uniprot.org/, https://www.genecards.org/ and https://www.ncbi.nlm.nih.gov/gene. To predict protein/gene interactions (Figure 3B) we used the STRING database (https://string-db.org/). To predict Shank2b protein structure (Figure S2A), we used the SMART database (http://smart.embl-heidelberg.de/).

Statistics: Differences between two groups were determined by independent (unpaired) two-sample *t* test using scipy.stats.ttest_ind in python. Differences between two groups within the same conditions before and after treatment were determined by paired *t* test using scipy.stats.ttest_rel in python. Differences between more than two groups were determined using one-way ANOVA followed by post hoc Tukey's test using scipy.stats.f_oneway and statsmodels.stats.multicomp.pairwise_tukeyhsd in python. Differences in RNAseq expression determined by the pairwise Wald test with Benjamini-Hochberg *p*-value correction using R and DESeq2 package. To determine whether observed overlaps between two gene sets are statistically significant, given the total background of 23180 genes, we performed a hypergeometric test using scipy.stats.hypergeom in python.

Supplementary Material

Refer to Web version on PubMed Central for supplementary material.

ACKNOWLEDGMENTS

We thank Geoff Meyerhof, Monique Smith, and Dhananjay Bambah-Mukku for comments on a previous version of this manuscript. We acknowledge funding from the Human Frontier Science Program Postdoctoral Fellowship LT0002/ 2022L (D.Z.), the Zuckerman STEM Israeli Postdoctoral Scholars Program (D.Z.), the European Research

Council (B.J.: ERC2021-CoG-101043615), the Einstein Foundation (B.J.: EPP-2017-413), the German Research Foundation (B.J.: DFG, project EXC-2049-390688087), the Alfried Krupp von Bohlen und Halbach Foundation (B.J.), the Searle Scholars Award (M.L.-B.), the Packard Foundation Fellowship (M.L.-B.), the Pew Biomedical Scholar Award (M.L.-B.), a McKnight Scholars Award (M.L-B.), the Sloan Research Fellowship (M.L.-B.), and the NIH New Innovator Award (M.L.-B.: DP2EY036251). This publication includes data generated at the UC San Diego IGM Genomics Center utilizing an Illumina NovaSeq 6000 that was purchased with funding from a National Institutes of Health SIG grant (#S10 OD026929).

Data and code availability

Data and code are available via NCBI BioProject: PRJNA1328681 and Figshare: https://doi.org/10.6084/m9.figshare.c.8035018.v1, links to which are also provided in the key resources table. Any additional information required to reanalyze the data reported in this paper is available from the lead contact upon request.

REFERENCES

1. Shaw E (1978). Schooling Fishes: The school, a truly egalitarian form of organization in which all members of the group are alike in influence, offers substantial benefits to its participants. Am. Sci 66, 166–175.
2. Krause J, and Ruxton GD (2002). Living in Groups (Oxford University Press).
3. Sumpter D, Buhl C, Biro D, and Couzin I (2008). Information transfer in moving animal groups. Theory Biosci. 127, 177–186. 10.1007/s12064-008-0040-1. [PubMed: 18458976]
4. Sumpter DJT (2010). Collective Animal Behavior (Princeton Univ. Press).
5. Couzin ID (2009). Collective cognition in animal groups. Trends Cogn. Sci 13, 36–43. 10.1016/j.tics.2008.10.002. [PubMed: 19058992]
6. Katz Y, Tunstrøm K, Ioannou CC, Huepe C, and Couzin ID (2011). Inferring the structure and dynamics of interactions in schooling fish. Proc. Natl. Acad. Sci. USA 108, 18720–18725. 10.1073/pnas.1107583108. [PubMed: 21795604]
7. Rosenthal SB, Twomey CR, Hartnett AT, Wu HS, and Couzin ID (2015). Revealing the hidden networks of interaction in mobile animal groups allows prediction of complex behavioral contagion. Proc. Natl. Acad. Sci. USA 112, 4690–4695. 10.1073/pnas.1420068112. [PubMed: 25825752]
8. Davidson JD, Sosna MMG, Twomey CR, Sridhar VH, Leblanc SP, and Couzin ID (2021). Collective detection based on visual information in animal groups. J. R. Soc. Interface 18, 20210142. 10.1098/rsif.2021.0142. [PubMed: 34229461]
9. Dreosti E, Lopes G, Kampff AR, and Wilson SW (2015). Development of social behavior in young zebrafish. Front. Neural Circuits 9, 39. 10.3389/fncir.2015.00039. [PubMed: 26347614]
10. Hinz RC, and de Polavieja GG (2017). Ontogeny of collective behavior reveals a simple attraction rule. Proc. Natl. Acad. Sci. USA 114, 2295–2300. 10.1073/pnas.1616926114. [PubMed: 28193864]
11. Larsch J, and Baier H (2018). Biological Motion as an Innate Perceptual Mechanism Driving Social Affiliation. Curr. Biol 28, 3523–3532.e4. 10.1016/j.cub.2018.09.014. [PubMed: 30393036]
12. Stednitz SJ, and Washbourne P (2020). Rapid Progressive Social Development of Zebrafish. Zebrafish 17, 11–17. 10.1089/zeb.2019.1815. [PubMed: 31930951]
13. Harpaz R, Nguyen MN, Bahl A, and Engert F (2021). Precise visuomotor transformations underlying collective behavior in larval zebrafish. Nat. Commun 12, 6578. 10.1038/s41467-021-26748-0. [PubMed: 34772934]
14. Zada D, Schulze L, Yu J-H, Tarabishi P, Napoli JL, Milan J, and Lovett-Barron M (2024). Development of neural circuits for social motion perception in schooling fish. Curr. Biol 34, 3380–3391.e5. 10.1016/j.cub.2024.06.049. [PubMed: 39025069]
15. Peça J, Feliciano C, Ting JT, Wang W, Wells MF, Venkatraman TN, Lascola CD, Fu Z, and Feng G (2011). Shank3 mutant mice display autistic-like behaviours and striatal dysfunction. Nature 472, 437–442. 10.1038/nature09965. [PubMed: 21423165]

16. Zaslavsky K, Zhang W-B, McCready FP, Rodrigues DC, Deneault E, Loo C, Zhao M, Ross PJ, El Hajjar J, Romm A, et al. (2019). SHANK2 mutations associated with autism spectrum disorder cause hyperconnectivity of human neurons. Nat. Neurosci 22, 556–564. 10.1038/s41593-019-0365-8. [PubMed: 30911184]

17. Giovedí S, Corradi A, Fassio A, and Benfenati F (2014). Involvement of synaptic genes in the pathogenesis of autism spectrum disorders: the case of synapsins. Front. Pediatr 2, 94. 10.3389/fped.2014.00094. [PubMed: 25237665]

18. Kilpinen H, Ylisaukko-Oja T, Hennah W, Palo OM, Varilo T, Vanhala R, Nieminen-von Wendt T, von Wendt L, Paunio T, and Peltonen L (2008). Association of DISC1 with autism and Asperger syndrome. Mol. Psychiatry 13, 187–196. 10.1038/sj.mp.4002031. [PubMed: 17579608]

19. Bradshaw NJ, and Porteous DJ (2012). DISC1-binding proteins in neural development, signalling and schizophrenia. Neuropharmacology 62, 1230–1241. 10.1016/j.neuropharm.2010.12.027. [PubMed: 21195721]

20. Landin J, Hovey D, Xu B, Lagman D, Zettergren A, Larhammar D, Kettunen P, and Westberg L (2020). Oxytocin Receptors Regulate Social Preference in Zebrafish. Sci. Rep 10, 5435. 10.1038/s41598-020-61073-4. [PubMed: 32214126]

21. Gemmer A, Mirkes K, Anneser L, Eilers T, Kibat C, Mathuru A, Ryu S, and Schuman E (2022). Oxytocin receptors influence the development and maintenance of social behavior in zebrafish (Danio rerio). Sci. Rep 12, 4322. 10.1038/s41598-022-07990-y. [PubMed: 35279678]

22. Anneser L, Gemmer A, Eilers T, Alcantara IC, Loos A-Y, Ryu S, and Schuman EM (2022). The neuropeptide Pth2 modulates social behavior and anxiety in zebrafish. iScience 25, 103868. 10.1016/j.isci.2022.103868. [PubMed: 35243231]

23. Thyme SB, Pieper LM, Li EH, Pandey S, Wang Y, Morris NS, Sha C, Choi JW, Herrera KJ, Soucy ER, et al. (2019). Phenotypic Landscape of Schizophrenia-Associated Genes Defines Candidates and Their Shared Functions. Cell 177, 478–491.e20. 10.1016/j.cell.2019.01.048. [PubMed: 30929901]

24. Weinschutz Mendes H, Neelakantan U, Liu Y, Fitzpatrick SE, Chen T, Wu W, Pruitt A, Jin DS, Jamadagni P, Carlson M, et al. (2023). High-throughput functional analysis of autism genes in zebrafish identifies convergence in dopaminergic and neuroimmune pathways. Cell Rep. 42, 112243. 10.1016/j.celrep.2023.112243. [PubMed: 36933215]

25. Tang W, Davidson JD, Zhang G, Conen KE, Fang J, Serluca F, Li J, Xiong X, Coble M, Tsai T, et al. (2020). Genetic Control of Collective Behavior in Zebrafish. iScience 23, 100942. 10.1016/j.isci.2020.100942. [PubMed: 32179471]

26. Miller N, and Gerlai R (2012). From Schooling to Shoaling: Patterns of Collective Motion in Zebrafish (Danio rerio). PLoS One 7, e48865. 10.1371/journal.pone.0048865. [PubMed: 23166599]

27. Schulze L, Henninger J, Kadobianskyi M, Chaigne T, Faustino AI, Hakiy N, Albadri S, Schuelke M, Maler L, Del Bene F, and Judkewitz B (2018). Transparent Danionella translucida as a genetically tractable vertebrate brain model. Nat. Methods 15, 977–983. 10.1038/s41592-018-0144-6. [PubMed: 30323353]

28. Kadobianskyi M, Schulze L, Schuelke M, and Judkewitz B (2019). Hybrid genome assembly and annotation of Danionella translucida. Sci. Data 6, 156. 10.1038/s41597-019-0161-z. [PubMed: 31451709]

29. Britz R, Conway KW, and Rüber L (2021). The emerging vertebrate model species for neurophysiological studies is Danionella cerebrum, new species (Teleostei: Cyprinidae). Sci. Rep 11, 18942. 10.1038/s41598-021-97600-0. [PubMed: 34556691]

30. Rajan G, Duroure K, and Del Bene F (2022). Danionella translucida, a tankful of new opportunities. In Laboratory Fish in Biomedical Research, D'angelo L and De Girolamo P, eds. (Elsevier), pp. 409–418. 10.1016/B978-0-12-821099-4.00017-1.

31. Lam P-Y (2022). Longitudinal in vivo imaging of adult Danionella cerebrum using standard confocal microscopy. Dis. Model. Mech 15, dmm049753. 10.1242/dmm.049753. [PubMed: 36398624]

32. Lee TJ, and Briggman KL (2023). Visually guided and context-dependent spatial navigation in the translucent fish Danionella cerebrum. Curr. Biol 33, 5467–5477.e4. 10.1016/j.cub.2023.11.030. [PubMed: 38070503]
33. Penalva-Tena A, Bedke J, Gaudin A, Barrios JP, Bertram EPL, and Douglass AD (2025). Oxytocin-mediated social preference and socially reinforced reward learning in the miniature fish Danionella cerebrum. Curr. Biol 35, 363–372.e3. 10.1016/j.cub.2024.11.037. [PubMed: 39732054]
34. Jo-Hsien Y, Napoli Julia L, and Matthew L-B (2024). Understanding collective behavior through neurobiology. Curr. Opin. Neurobiol 86, 102866. 10.1016/j.conb.2024.102866. [PubMed: 38852986]
35. Groneberg AH, Dressler LE, Kadobianskyi M, Müller J, and Judkewitz B (2024). Development of sound production in Danionella cerebrum. J. Exp. Biol 227, jeb247782. 10.1242/jeb.247782. [PubMed: 39189063]
36. Weber MD, Godbout JP, and Sheridan JF (2017). Repeated Social Defeat, Neuroinflammation, and Behavior: Monocytes Carry the Signal. Neuropsychopharmacology 42, 46–61. 10.1038/npp.2016.102. [PubMed: 27319971]
37. Nakagawa Y, and Chiba K (2016). Involvement of Neuroinflammation during Brain Development in Social Cognitive Deficits in Autism Spectrum Disorder and Schizophrenia. J. Pharmacol. Exp. Ther 358, 504–515. 10.1124/jpet.116.234476. [PubMed: 27384073]
38. Kareklas K, Teles MC, Dreosti E, and Oliveira RF (2023). Autism-associated gene shank3 is necessary for social contagion in zebrafish. Mol. Autism 14, 23. 10.1186/s13229-023-00555-4. [PubMed: 37391856]
39. Kroll F, Powell GT, Ghosh M, Gestri G, Antinucci P, Hearn TJ, Tunbak H, Lim S, Dennis HW, Fernandez JM, et al. (2021). A simple and effective F0 knockout method for rapid screening of behaviour and other complex phenotypes. eLife 10, e59683. 10.7554/eLife.59683. [PubMed: 33416493]
40. Debaenst S, Jarayseh T, De Saffel H, Bek JW, Boone M, Josipovic I, Kibleur P, Kwon RY, Coucke PJ, and Willaert A (2025). Crispant analysis in zebrafish as a tool for rapid functional screening of disease-causing genes for bone fragility. eLife 13, RP100060. 10.7554/eLife.100060. [PubMed: 39817421]
41. Tropea D, Hardingham N, Millar K, and Fox K (2018). Mechanisms underlying the role of DISC1 in synaptic plasticity. J. Physiol 596, 2747–2771. 10.1113/JP274330. [PubMed: 30008190]
42. Naisbitt S, Kim E, Tu JC, Xiao B, Sala C, Valtschanoff J, Weinberg RJ, Worley PF, and Sheng M (1999). Shank, a novel family of postsynaptic density proteins that binds to the NMDA receptor/PSD-95/GKAP complex and cortactin. Neuron 23, 569–582. 10.1016/s0896-6273(00)80809-0. [PubMed: 10433268]
43. Ferreira A, Chin L-S, Li L, Lanier LM, Kosik KS, and Greengard P (1998). Distinct Roles of Synapsin I and Synapsin II during Neuronal Development. Mol. Med 4, 22–28. 10.1007/BF03401726. [PubMed: 9513186]
44. Choi HMT, Schwarzkopf M, Fornace ME, Acharya A, Artavanis G, Stegmaier J, Cunha A, and Pierce NA (2018). Third-generation in situ hybridization chain reaction: multiplexed, quantitative, sensitive, versatile, robust. Dev. Camb. Engl 145, dev165753. 10.1242/dev.165753.
45. Guang S, Pang N, Deng X, Yang L, He F, Wu L, Chen C, Yin F, and Peng J (2018). Synaptopathology Involved in Autism Spectrum Disorder. Front. Cell. Neurosci 12, 470. 10.3389/fncel.2018.00470. [PubMed: 30627085]
46. Guillaumond F, Dardente H, Giguère V, and Cermakian N (2005). Differential control of Bmal1 circadian transcription by REV-ERB and ROR nuclear receptors. J. Biol. Rhythms 20, 391–403. 10.1177/0748730405277232. [PubMed: 16267379]
47. Bozek K, Relógio A, Kielbasa SM, Heine M, Dame C, Kramer A, and Herzel H (2009). Regulation of clock-controlled genes in mammals. PLoS One 4, e4882. 10.1371/journal.pone.0004882. [PubMed: 19287494]
48. Honma S, Kawamoto T, Takagi Y, Fujimoto K, Sato F, Noshiro M, Kato Y, and Honma K.i. (2002). Dec1 and Dec2 are regulators of the mammalian molecular clock. Nature 419, 841–844. 10.1038/nature01123. [PubMed: 12397359]

49. Drolet DW, Scully KM, Simmons DM, Wegner M, Chu KT, Swanson LW, and Rosenfeld MG (1991). TEF, a transcription factor expressed specifically in the anterior pituitary during embryogenesis, defines a new class of leucine zipper proteins. Genes Dev. 5, 1739–1753. 10.1101/gad.5.10.1739. [PubMed: 1916262]
50. Bianco AC, and da Conceição RR (2018). The Deiodinase Trio and Thyroid Hormone Signaling. Methods Mol. Biol. Clifton NJ 1801, 67–83. 10.1007/978-1-4939-7902-8_8.
51. Dugas JC, Ibrahim A, and Barres BA (2012). The T3-induced gene KLF9 regulates oligodendrocyte differentiation and myelin regeneration. Mol. Cell. Neurosci 50, 45–57. 10.1016/j.mcn.2012.03.007. [PubMed: 22472204]
52. Ogawa S, Lee Y-A, Yamaguchi Y, Shibata Y, and Goto Y (2017). Associations of acute and chronic stress hormones with cognitive functions in autism spectrum disorder. Neuroscience 343, 229–239. 10.1016/j.neuroscience.2016.12.003. [PubMed: 27956063]
53. Numakawa T, Adachi N, Richards M, Chiba S, and Kunugi H (2012). The influence of glucocorticoids on neuronal survival and synaptic function. Biomol. Concepts 3, 495–504. 10.1515/bmc-2012-0012. [PubMed: 25436554]
54. Raudensky J, and Yamamoto BK (2007). Effects of chronic unpredictable stress and methamphetamine on hippocampal glutamate function. Brain Res. 1135, 129–135. 10.1016/j.brainres.2006.12.002. [PubMed: 17198685]
55. Ramos-Brossier M, Romeo-Guitart D, Lanté F, Boitez V, Mailliet F, Saha S, Rivagorda M, Siopi E, Nemazanyy I, Leroy C, et al. (2024). Slc20a1 and Slc20a2 regulate neuronal plasticity and cognition independently of their phosphate transport ability. Cell Death Dis. 15, 20. 10.1038/s41419-023-06292-z. [PubMed: 38195526]
56. Gavaldà A, Benyassi A, Arancibia S, and Armario A (1993). Chronic but not acute exposure to stress is associated with hypothalamic vasoactive intestinal polypeptide (VIP) release into median eminence. J. Neuroendocrinol 5, 421–425. 10.1111/j.1365-2826.1993.tb00503.x. [PubMed: 8401565]
57. Markova N, Chernopiatko A, Schroeter CA, Malin D, Kubatiev A, Bachurin S, Costa-Nunes J, Steinbusch HMW, and Strekalova T (2013). Hippocampal gene expression of deiodinases 2 and 3 and effects of 3,5-diiodo-L-thyronine T2 in mouse depression paradigms. BioMed Res. Int 2013, 565218. 10.1155/2013/565218. [PubMed: 24386638]
58. Suzuki-Yagawa Y, Kawakami K, and Nagano K (1992). Housekeeping Na,K-ATPase alpha 1 subunit gene promoter is composed of multiple cis elements to which common and cell type-specific factors bind. Mol. Cell Biol 12, 4046–4055. 10.1128/mcb.12.9.4046-4055.1992. [PubMed: 1324413]
59. Lomberk G, and Urrutia R (2005). The family feud: turning off Sp1 by Sp1-like KLF proteins. Biochem. J 392, 1–11. 10.1042/BJ20051234. [PubMed: 16266294]
60. Zhang Y, Xue Y, Cao C, Huang J, Hong Q, Hai T, Jia Q, Wang X, Qin G, Yao J, et al. (2017). Thyroid hormone regulates hematopoiesis via the TR-KLF9 axis. Blood 130, 2161–2170. 10.1182/blood-2017-05-783043. [PubMed: 28972010]
61. Cvoro A, Devito L, Milton FA, Noli L, Zhang A, Filippi C, Sakai K, Suh JH, H Sieglaff D, Dhawan A, et al. (2015). A thyroid hormone receptor/KLF9 axis in human hepatocytes and pluripotent stem cells. Stem Cell. 33, 416–428. 10.1002/stem.1875.
62. Zada D, Tovin A, Lerer-Goldshtein T, Vatine GD, and Appelbaum L (2014). Altered behavioral performance and live imaging of circuit-specific neural deficiencies in a zebrafish model for psychomotor retardation. PLoS Genet. 10, e1004615. 10.1371/journal.pgen.1004615. [PubMed: 25255244]
63. Robinson GE, Fernald RD, and Clayton DF (2008). Genes and social behavior. Science 322, 896–900. 10.1126/science.1159277. [PubMed: 18988841]
64. Gatto CL, and Broadie K (2010). Genetic controls balancing excitatory and inhibitory synaptogenesis in neurodevelopmental disorder models. Front. Synaptic Neurosci 2, 4. 10.3389/fnsyn.2010.00004. [PubMed: 21423490]
65. Bernal J (2007). Thyroid hormone receptors in brain development and function. Nat. Clin. Pract. Endocrinol. Metab 3, 249–259. 10.1038/ncpendmet0424. [PubMed: 17315033]

66. Chang JT, Lowery LA, and Sive H (2012). Multiple roles for the Na,KATPase subunits, Atp1a1 and Fxyd1, during brain ventricle development. Dev. Biol 368, 312–322. 10.1016/j.ydbio.2012.05.034. [PubMed: 22683378]

67. Logan RW, and McClung CA (2019). Rhythms of life: circadian disruption and brain disorders across the lifespan. Nat. Rev. Neurosci 20, 49–65. 10.1038/s41583-018-0088-y. [PubMed: 30459365]

68. Walker WH, Walton JC, DeVries AC, and Nelson RJ (2020). Circadian rhythm disruption and mental health. Transl. Psychiatry 10, 28. 10.1038/s41398-020-0694-0. [PubMed: 32066704]

69. Mishra A, Lin H, Singla R, Le N, Oraebosi M, Liu D, and Cao R (2024). Circadian desynchrony in early life leads to enduring autistic-like behavioral changes in adulthood. Commun. Biol 7, 1485. 10.1038/s42003-024-07131-3. [PubMed: 39528720]

70. Gonçalves FB, Gonçalves BSB, Cavalcante JS, and Azevedo CVM (2020). Aging-related changes on social synchronization of circadian activity rhythm in a diurnal primate (Callithrix jacchus). Chronobiol. Int 37, 980–992. 10.1080/07420528.2020.1773495. [PubMed: 32573282]

71. Paul MJ, Indic P, and Schwartz WJ (2015). Social synchronization of circadian rhythmicity in female mice depends on the number of cohabiting animals. Biol. Lett 11, 20150204. 10.1098/rsbl.2015.0204. [PubMed: 26063754]

72. Fuchikawa T, Eban-Rothschild A, Nagari M, Shemesh Y, and Bloch G (2016). Potent social synchronization can override photic entrainment of circadian rhythms. Nat. Commun 7, 11662. 10.1038/ncomms11662. [PubMed: 27210069]

73. Teo CH, Soga T, and Parhar IS (2017). Social Isolation Modulates CLOCK Protein and Beta-Catenin Expression Pattern in Gonadotropin-Inhibitory Hormone Neurons in Male Rats. Front. Endocrinol 8, 225. 10.3389/fendo.2017.00225.

74. Kaushal N, Nair D, Gozal D, and Ramesh V (2012). Socially isolated mice exhibit a blunted homeostatic sleep response to acute sleep deprivation compared to socially paired mice. Brain Res. 1454, 65–79. 10.1016/j.brainres.2012.03.019. [PubMed: 22498175]

75. Favreau A, Richard-Yris M-A, Bertin A, Houdelier C, and Lumineau S (2009). Social influences on circadian behavioural rhythms in vertebrates. Anim. Behav 77, 983–989. 10.1016/j.anbehav.2009.01.004.

76. Hagenauer MH, Perryman JI, Lee TM, and Carskadon MA (2009). Adolescent changes in the homeostatic and circadian regulation of sleep. Dev. Neurosci 31, 276–284. 10.1159/000216538. [PubMed: 19546564]

77. Tesfaye R, Huguet G, Schmilovich Z, Renne T, Loum MA, Douard E, Saci Z, Jean-Louis M, Martineau JL, Whelan R, et al. (2022). Investigating the contributions of circadian pathway and insomnia risk genes to autism and sleep disturbances. Transl. Psychiatry 12, 424. 10.1038/s41398-022-02188-2. [PubMed: 36192372]

78. Friesema ECH, Ganguly S, Abdalla A, Manning Fox JE, Halestrap AP, and Visser TJ (2003). Identification of Monocarboxylate Transporter 8 as a Specific Thyroid Hormone Transporter. J. Biol. Chem 278, 40128–40135. 10.1074/jbc.M300909200. [PubMed: 12871948]

79. Getahun D, Jacobsen SJ, Fassett MJ, Wing DA, Xiang AH, Chiu VY, and Peltier MR (2018). Association between maternal hypothyroidism and autism spectrum disorders in children. Pediatr. Res 83, 580–588. 10.1038/pr.2017.308. [PubMed: 29244797]

80. Williams GR (2008). Neurodevelopmental and neurophysiological actions of thyroid hormone. J. Neuroendocrinol 20, 784–794. 10.1111/j.1365-2826.2008.01733.x. [PubMed: 18601701]

81. St-Cyr S, Abuaish S, Welch KC, and McGowan PO (2018). Maternal predator odour exposure programs metabolic responses in adult offspring. Sci. Rep 8, 8077. 10.1038/s41598-018-26462-w. [PubMed: 29799024]

82. Tata JR (2006). Amphibian metamorphosis as a model for the developmental actions of thyroid hormone. Mol. Cell. Endocrinol 246, 10–20. 10.1016/j.mce.2005.11.024. [PubMed: 16413959]

83. Aman AJ, Kim M, Saunders LM, and Parichy DM (2021). Thyroid hormone regulates abrupt skin morphogenesis during zebrafish postembryonic development. Dev. Biol 477, 205–218. 10.1016/j.ydbio.2021.05.019. [PubMed: 34089732]

84. Bassett JHD, and Williams GR (2016). Role of Thyroid Hormones in Skeletal Development and Bone Maintenance. Endocr. Rev 37, 135–187. 10.1210/er.2015-1106. [PubMed: 26862888]

85. Zhao J, Guo X, Du Y, Han Y, Wang Y, Li L, Qian J, Li M, Wu H, Golden T, and Wu N (2016). Correlative study of peripheral *ATP1A1* gene expression level to anxiety severity score on major depressive disorder patients. J. Basic Clin. Physiol. Pharmacol 27, 563–567. 10.1515/jbcpp-2015-0148. [PubMed: 27487491]
86. Biondo ED, Spontarelli K, Ababioh G, Méndez L, and Artigas P (2021). Diseases caused by mutations in the Na^+/K^+ pump α1 gene *ATP1A1*. Am. J. Physiol. Cell Physiol 321, C394–C408. 10.1152/ajpcell.00059.2021. [PubMed: 34232746]
87. Zhang J, Piontek J, Wolburg H, Piehl C, Liss M, Otten C, Christ A, Willnow TE, Blasig IE, and Abdelilah-Seyfried S (2010). Establishment of a neuroepithelial barrier by Claudin5a is essential for zebrafish brain ventricular lumen expansion. Proc. Natl. Acad. Sci. USA 107, 1425–1430. 10.1073/pnas.0911996107. [PubMed: 20080584]
88. Jeong I, Andreassen SN, Hoang L, Poulain M, Seo Y, Park H-C, Fürthauer M, MacAulay N, and Jurisch-Yaksi N (2024). The evolutionarily conserved choroid plexus contributes to the homeostasis of brain ventricles in zebrafish. Cell Rep. 43, 114331. 10.1016/j.cel-rep.2024.114331. [PubMed: 38843394]
89. Scobie KN, Hall BJ, Wilke SA, Klemenhagen KC, Fujii-Kuriyama Y, Ghosh A, Hen R, and Sahay A (2009). Krüppel-like factor 9 is necessary for late-phase neuronal maturation in the developing dentate gyrus and during adult hippocampal neurogenesis. J. Neurosci 29, 9875–9887. 10.1523/JNEUROSCI.2260-09.2009. [PubMed: 19657039]
90. Guo N, McDermott KD, Shih Y-T, Zanga H, Ghosh D, Herber C, Meara WR, Coleman J, Zagouras A, Wong LP, et al. (2022). Transcriptional regulation of neural stem cell expansion in the adult hippocampus. eLife 11, e72195. 10.7554/eLife.72195. [PubMed: 34982030]
91. Bass AH, and Perelmuter JT (2024). Danionella fishes. Nat Methods 21, 1767–1769. 10.1038/s41592-024-02433-0. [PubMed: 39384984]
92. Pereira TD, Tabris N, Matsliah A, Turner DM, Li J, Ravindranath S, Papadoyannis ES, Normand E, Deutsch DS, Wang ZY, et al. (2022). SLEAP: A deep learning system for multi-animal pose tracking. Nat. Methods 19, 486–495. 10.1038/s41592-022-01426-1. [PubMed: 35379947]
93. Lopes G, Farrell K, Horrocks EA, Lee C-Y, Morimoto MM, Muzzu T, Papanikolaou A, Rodrigues FR, Wheatcroft T, Zucca S, et al. (2021). Creating and controlling visual environments using BonVision. eLife 10, e65541. 10.7554/eLife.65541. [PubMed: 33880991]
94. Love MI, Huber W, and Anders S (2014). Moderated estimation of fold change and dispersion for RNA-seq data with DESeq2. Genome Biol. 15, 550. 10.1186/s13059-014-0550-8. [PubMed: 25516281]
95. Admati I, Wasserman-Bartov T, Tovin A, Rozenblat R, Blitz E, Zada D, Lerer-Goldshtein T, and Appelbaum L (2020). Neural Alterations and Hyperactivity of the Hypothalamic-Pituitary-Thyroid Axis in Oatp1c1 Deficiency. Thyroid 30, 161–174. 10.1089/thy.2019.0320. [PubMed: 31797746]
96. Guilbeault NC, Guerguiev J, Martin M, Tate I, and Thiele TR (2021). BonZeb: open-source, modular software tools for high-resolution zebrafish tracking and analysis. Sci. Rep 11, 8148. 10.1038/s41598-021-85896-x. [PubMed: 33854104]
97. Cook VANO, Groneberg AH, Hoffmann M, Kadobianskyi M, Veith J, Schulze L, Henninger J, Britz R, and Judkewitz B (2024). Ultrafast sound production mechanism in one of the smallest vertebrates. Proc. Natl. Acad. Sci 121, e2314017121. 10.1073/pnas.2314017121. [PubMed: 38408231]
98. Patro R, Duggal G, Love MI, Irizarry RA, and Kingsford C (2017). Salmon provides fast and bias-aware quantification of transcript expression. Nat. Methods 14, 417–419. 10.1038/nmeth.4197. [PubMed: 28263959]
99. Young MD, Wakefield MJ, Smyth GK, and Oshlack A (2010). Gene ontology analysis for RNA-seq: accounting for selection bias. Genome Biol. 11, R14. 10.1186/gb-2010-11-2-r14. [PubMed: 20132535]

Highlights

- Measuring brain transcriptomes of the schooling fish *Danionella cerebrum*
- Schooling is impaired in crispants of ASD-related genes
- Identifying common patterns of gene expression across models of impaired schooling
- Genetic and pharmacological manipulations link a thyroid-*klf9*-*atp1a1* pathway to schooling

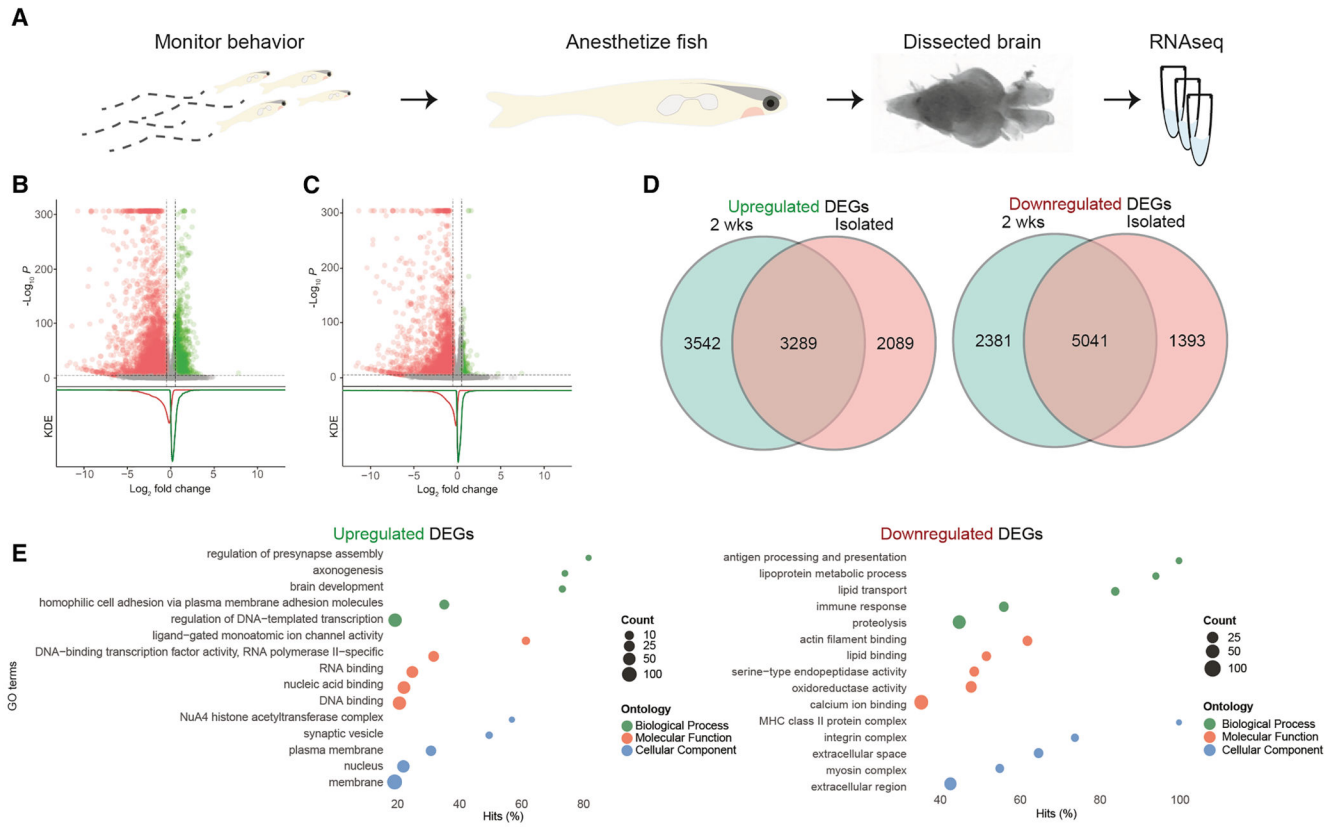

Figure 1. Brain RNA sequencing identifies gene expression associated with social development

(A) Schematic illustration of the experimental procedure. A group of four fish was monitored for schooling behavior. Immediately afterward, the fish were anesthetized, whole brains dissected, and RNA sequencing was performed.

(B) Volcano plot for DEGs between two- and six-week-old brains.

(C) Volcano plot for DEGs between socially raised and socially isolated six-week-old brains. Dashed lines and colored circles indicate DEGs with $p < 0.05$ and absolute logFC > 0.5. p values below 1e-300 are set to zero.

(D) Venn diagram of up- and downregulated genes in two-week-old fish and socially isolated six-week-old fish, relative to six-week-old controls (logFC > 0, $p < 0.05$).

(E) GO terms overrepresented in the overlapping genes shown in (D).

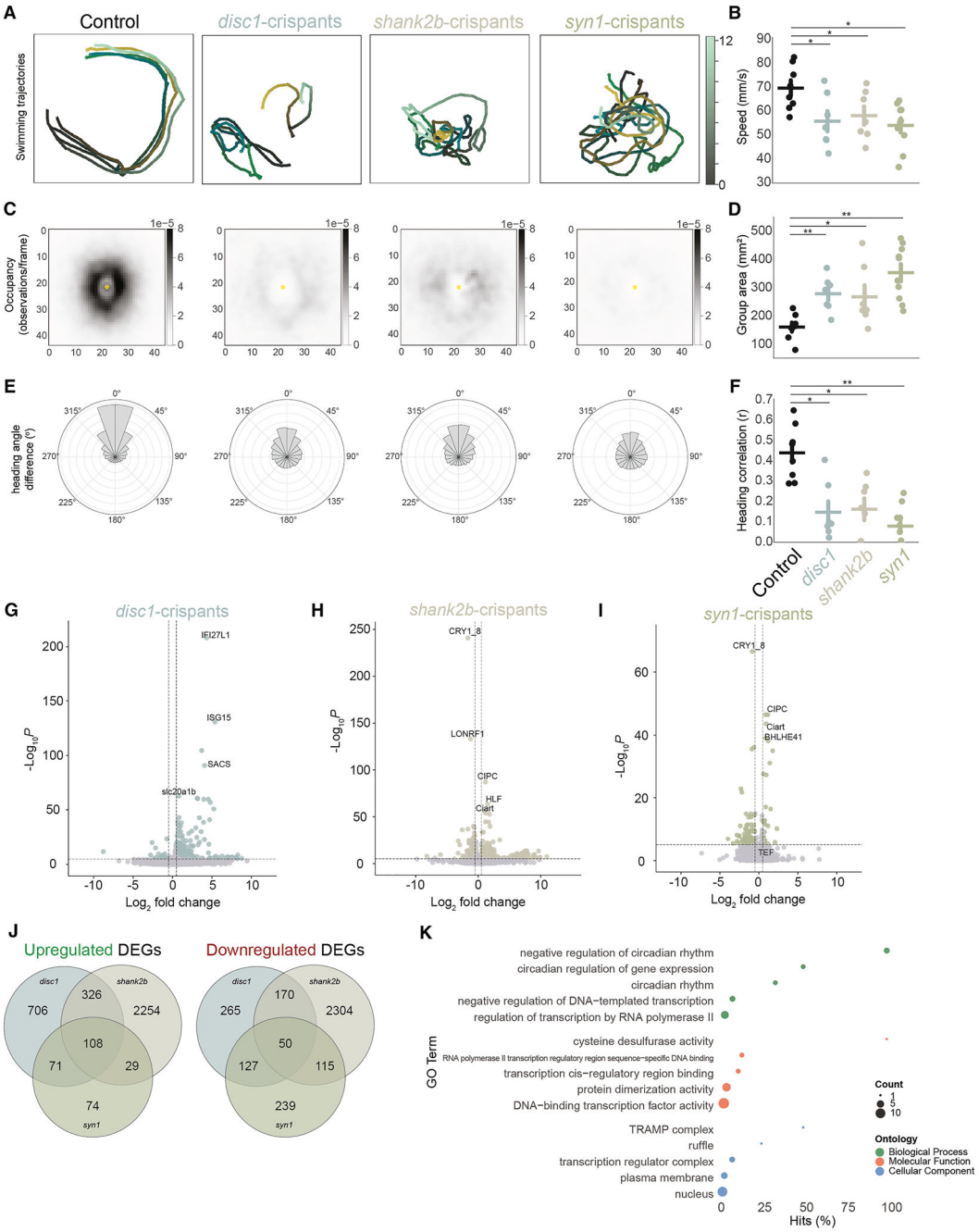

Figure 2. ASD-related crispants exhibit reduced schooling and altered brain transcriptomic profiles

(A) Example of group movement for *D. cerebrum* of different genotypes (left to right: Cas9-only control, *disc1*-, *shank2b*-, and *syn1*-crispants), swimming in a 300-mm diameter arena. Projection of tracked movement over 12 s, with each fish shown in a different color. (B) Mean speed. Individual data points are the means of the four fish in the group. Control groups compared with *disc1*-crispants ($t = 2.6$, $p = 0.02$, df = 13.0), *shank2b*-crispants ($t = 2.3$, $p = 0.03$, df = 13.0), and *syn1*-crispants ($t = 3.5$, $p = 0.002$, df = 16.0).

(C) Egocentric occupancy heatmaps, for groups of four fish (left to right: Cas9-only control, *disc1*-, *shank2b*-, and *syn1*-crispants). Darker colors indicate more observations of fish at this position relative to the focal individual (yellow dot); average of all timepoints across subjects).

(D) Mean group area, comparing groups of four fish. Control-groups compared with *disc1*-crispants ($t = -4.2$, $p = 0.00092$, df = 13.0), *shank2b*-crispants ($t = -2.6$, $p = 0.022$, df = 13.0), *syn1*-crispants ($t = -5.2$, $p = 8.4 \times 10^{-5}$, df = 16.0).

(E) Polar histograms of nearest-neighbor angle differences, for groups of four fish (left to right: Cas9-only control, *disc1*-, *shank2b*-, and *syn1*-crispants). Observations around 0° / 360° indicate aligned neighbors. Histogram of all timepoints across all fish.

(F) Mean of pairwise heading direction correlation coefficients amongst all fish, comparing between groups of four fish. Control-groups compared with *disc1*- crispants ($t = 4.1$, $p = 0.0012$, df = 13.0), *shank2b*-crispants ($t = 3.9$, $p = 0.0018$, df = 13.0), and *syn1*-crispants ($t = 6.7$, $p = 4.6 \times 10^{-6}$, df = 16.0).

(G–I) Volcano plots of differential expression in the *disc1*- (G), *shank2b*- (H), and *syn1*- (I) crispants relative to the Cas9-only controls. Colored circles indicate genes with $p < 1e\text{-}6$ and absolute logFC > 0.5. *p* values below 1e-300 are set to zero. Top five most significant DEGs are indicated on each plot.

(J) Venn diagram of the overlap between DEGs that are upregulated (left) or downregulated (right) in all three crispants.

(K) Overrepresented GO terms in the genes that are differentially expressed in all three crispants. (A–F) $N = 8$, 7, 7, and 10 groups for Cas9-only control, *disc1*-, *shank2b*-, and *syn1*-crispants, respectively $^{*}p < 0.05$ and $^{**}p < 0.001$, determined by unpaired two-sample *t* test. Mean ± SEM with individual points is shown (B, D, and F).

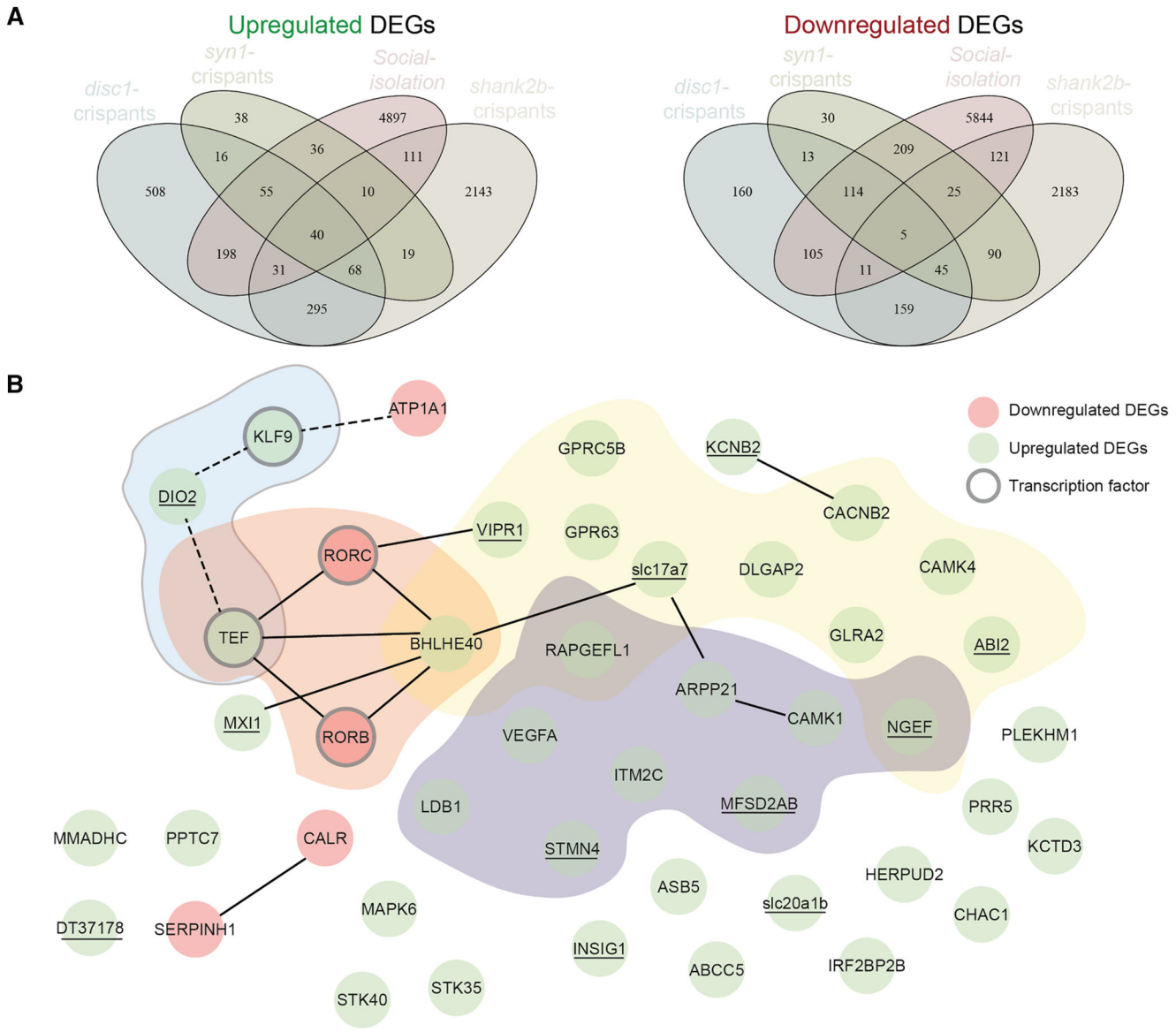

Figure 3. Transcriptomic comparison across non-schooling models

(A) Venn diagrams representing the overlap of genes shared among *disc1*-, *shank2b*-, and *syn1*-crispants and isolated *D. cerebrum*.

(B) A diagram illustrating the connections between the 45 converging differentially expressed genes (DEGs). Underlined gene names indicate genes excluded after further analysis of DEGs overlapping in two-week-old fish and socially isolated six-week-old fish (relative to six-week-old controls), as well as from the set of overlapping DEGs across all three crispants compared to Cas9-only controls. Solid lines represent protein interactions based on the STRING database. The colored background highlights gene groups associated with thyroid (blue), circadian rhythm (red), synaptic structure and function (yellow), and nervous system development (purple). Green circles indicate genes with increased expression in schooling-deficient fish, whereas red circles show reduced expression. Gray

outlines indicate transcription factors. Dashed lines represent a pathway of interest, which we further examine in Figure 4.

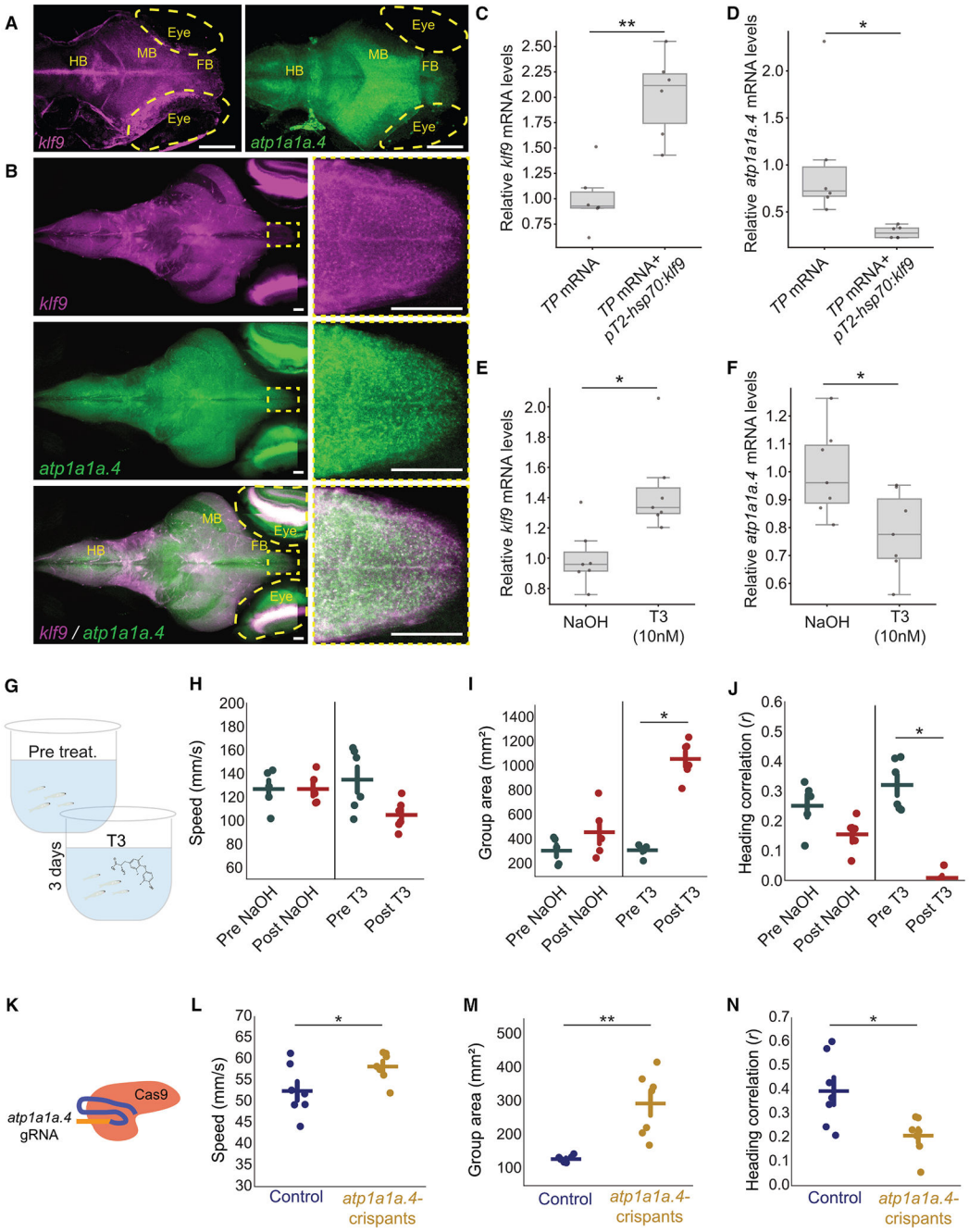

Figure 4. Thyroid-*klf9-atp1a1a.4* pathway regulates *D. cerebrum* schooling

(A and B) Whole-mount HCR-FISH experiments revealed the spatial mRNA expression of *klf9* (magenta) and *atp1a1a.4* (green) in two-week-old (A) and adult (B) *D. cerebrum* (dorsal view). Scale bars, 50 μm. A zoomed-in (yellow dashed boxes) view of the anterior parvocellular nucleus of the preoptic area shows cells co-expressing *klf9* and *atp1a1a.4* (white, right panels in B). FB, forebrain; MB, midbrain; and HB, hindbrain.

(C and D) Relative mRNA expression levels of *klf9* and *atp1a1a.4* in 6 dpf *pTol2-hsp70:klf9+TP* mRNA-injected ($N = 6$) and *TP* mRNA-injected larvae ($N = 6$), following heat shock.

(E and F) Relative mRNA expression levels of *klf9* and *atp1a1a.4* in NaOH- ($N = 6$) and T3-treated ($N = 6$) WT 6 dpf larvae.

(G–J) Thyroid hormone administration (T3 [50 nM, 100 nM] or vehicle control [5×10^{-6} M NaOH]) reduces schooling behavior.

(H) Mean speed. Individual data points are the means of the four fish in the group.

(I) Mean group area, comparing groups of four fish (Pre-T3: 315.7 ± 41.2 mm^2; Post-T3: 1063.64 ± 141.4 mm^2, $t = -11.3$, $p = 9 \times 10^{-5}$).

(J) Mean of pairwise heading direction correlation coefficients among all fish, comparing between groups of four fish (Pre-T3: $r = 0.32 \pm 0.07$; Post-T3: $r = 0.008 \pm 0.019$, $t = 9.2$, $p = 0.0002$).

(K–N) *atp1a1a.4* crispants exhibit reduced schooling behavior compared to Cas9-only injected fish (control).

(L) Mean speed, individual data points are means of the four fish in the group (control: 52.5 ± 5.7 mm/s, *atp1a1a.4*: 58.23 ± 5.1 mm/s, $t = -2.2$, p value = 0.046).

(M) Mean group area, comparing groups of four fish (control: 129.0 ± 8.9 mm^2, *atp1a1a.4*: 294.6 ± 86.5 mm^2, $t = -4.6$, p value = 0.0005).

(N) Mean of pairwise heading direction correlation coefficients among all fish, comparing between groups of four fish (control: $r = 0.39 \pm 0.14$, *atp1a1a.4*: $r = 0.2 \pm 0.07$, $t = 2.9$, p value = 0.013). $N = 6$ for (C–F), 6 T3-and 5 NaOH-treated fish in (H–J), and 7 for both groups in (L–N). *$p < 0.05$ and **$p < 0.001$, determined by unpaired two-sample t test (C–F, L, and N) or paired t test (H–J). Boxplots (C–F) or Mean ± SEM (H–J and L–N) with individual points are shown.

KEY RESOURCES TABLE

REAGENT or RESOURCE	SOURCE	IDENTIFIER
Chemicals, peptides, and recombinant proteins		
Alt-R S.p. Cas9 Nuclease V3	IDT	https://www.idtdna.com/page
Gateway LR Clonase reaction	Invitrogen™	11791020
Restriction enzymes	NEB	https://www.neb.com/en/products/restriction-endonucleases
T3	Sigma-Aldrich	T2877
RIMS (EasyIndex custom RI 1.465)	LifeCanvas Technologies	https://lifecanvastech.com/shop/easyindex/
Critical commercial assays		
Direct-zol RNA MiniPrep kit	Zymo Research Corporation	R2053
qScript cDNA SuperMix	Quanta BioSciences	95048
PerfeCTa SYBR Green FastMix	Quanta BioSciences	95072
HCR 3.0 hairpin amplifiers	Molecular Instruments	https://www.molecularinstruments.com
Deposited data		
Raw sequencing data	NCBI SRA	https://www.ncbi.nlm.nih.gov/bioproject/PRJNA1328681
Updated genetic annotation	figshare	https://doi.org/10.6084/m9.figshare.c.8035018.v1
Gene count tables	figshare	https://doi.org/10.6084/m9.figshare.c.8035018.v1
Data analysis code	figshare	https://doi.org/10.6084/m9.figshare.c.8035018.v1
Experimental models: Organisms/strains		
Danionella cerebrum: wild type	Judkewitz and Douglass Labs	NA
Oligonucleotides		
Primers	IDT	https://www.idtdna.com/page
sgRNA	IDT	https://www.idtdna.com/page
oPools of gene probes for HCR	IDT	https://www.idtdna.com/page
Primers for genomic *disc1*: 5′-TTCAAATTGTAGAGTCTGCTTTAAG-3′ and 5′-GTGGTGATCACAGGAGGAGT-3′	This paper	N/A
Primers for genomic *shank2b*: 5′-ATGATGCCACGAAGCCCCAT-3′ and 5′-GAGATCTCCACCACTCACTTCT-3′	This paper	N/A
Primers for genomic *syn1*: 5′-CAGTCCGTCTGCTGGTCATCA-3′ and 5′-GTGTAATTTGTCCTGCAAAACAGGG-3′	This paper	N/A
Primers for genomic *atp1a1a.4*: 5′-GGCTGCAACTTCAGATGATGG-3′ and 5′-AGCTGCAAGTTCCTTGACGA-3′	This paper	N/A
Primers for RT-qPCR *klf9*: 5′-GTGGCAAAGTCTACGGAAAATC-3′ and 5′-GGTATGTGTACGGAAGTGTCG-3′	This paper	N/A

REAGENT or RESOURCE	SOURCE	IDENTIFIER
Primers for RT-qPCR *atp1a1a.4*: 5′-ACCACAAGTTGACACTCGATG-3′ and 5′-GAACTTGACCCATTCTGGAGTAG-3′	This paper	N/A
Primers for RT-qPCR *mrpl13*: 5′-AGAGAAGGCGATATGTTTGGTG-3′ and 5′-CCTGGGAAAATCGCTTCATTG-3′	This paper	N/A
Guide for *disc1* (sgRNA site: 5′-CTCAAGAGTTGTGTGACAAG-3′)	This paper	N/A
Guide for *shank2b* (sgRNA site: 5′-GACAATCTGTGTGGTTATCC-3′)	This paper	N/A
Guide for *syn1* (sgRNA site: 5′-GAGATCGCCCATATATCCAT-3′)	This paper	N/A
Guide for *atp1a1a.4* (sgRNA site: 5′-AGTATGGTACTGACCTCACC-3′)	This paper	N/A
Recombinant DNA		
pTol2-hsp70:klf9	This paper	N/A
pME-MCS	Tol2Kit	ZFIN: ZDB-PUB-071023-14
p5E-hsp70L	Tol2Kit	ZFIN: ZDB-PUB-071023-14
p3E-polyA	Tol2Kit	ZFIN: ZDB-PUB-071023-14
pDestTol2CG2	Tol2Kit	ZFIN: ZDB-PUB-071023-14
Software and algorithms		
SLEAP 1.3	Pereira et al.[92]	https://github.com/talmolab/sleap
BonsaiRx	Lopes et al.[93]	https://bonsai-rx.org/
DESeq2	Love et al.[94]	https://bioconductor.org/packages/DESeq2/
Other		
FemtoJet 4i microinjector	Eppendorf™	5252000021
Pico Projector	AnyBeam	HD301M1-H2
Infrared light	CMVision Technologies Inc.	CM-IR130-850NM
Camera	FLIR Grasshopper	#33-534
8 mm F/1.8 lens	Edmund Optics	#15-626
Long-pass filter	Edmund Optics	#12-767